Journal of Computational Biophysics and Chemistry

Research

Cite This: *J. Comput. Biophys. Chem.* **2025**, *24* (5), 535–556

Structure-Based Design of Potential anti-Dengue Compounds against the Envelope Glycoprotein of Dengue 2 Virus

George Hanson[*,¶], Nana Effiansah Asmah[†,‖], Millicent Abena Adzagbo[†,**], Gifty Adobea Nyarko[†,††], Emmanuel Bronii[‡,‡‡], Michael D. Wilson[§,§§,¶¶] and Samuel K. Kwofie[†,‖ ‖]

[*]*Department of Parasitology, Noguchi Memorial Institute for Medical Research, College of Health Sciences, University of Ghana, Legon, Accra, Ghana*

[†]*Department of Biomedical Engineering, School of Engineering Sciences, College of Basic & Applied Sciences, University of Ghana, Legon LG 77, Accra, Ghana*

[‡]*Department of Medicine, Loyola University Medical Center, Loyola University Chicago, Maywood, IL 60153, USA*

[§]*Department of Parasitology, Noguchi Memorial Institute for Medical Research, College of Health Sciences, University of Ghana, Legon, Accra, Ghana*

[¶]*gehanson@noguchi.ug.edu.gh*

[‖]*Nanaeffiansahasmah@gmail.com*

[**]*millicentadzagbo@gmail.com*

[††]*Giftyn18@gmail.com*

[‡‡]*ebroni@luc.edu*

[§§]*mwilson@noguchi.ug.edu.gh*

[¶¶]*Deceased*

[‖ ‖]Corresponding author. E-mail: *skkwofie@ug.edu.gh*

ABSTRACT: The spread of dengue fever has resulted in several deaths for which no drug is currently efficacious. A potential target for the development of an antiviral drug that prevents conformational changes and interferes with membrane fusion is the Dengue β-OG binding pocket. This study aimed to identify potential natural product leads with the propensity to inhibit the envelope protein. Three known inhibitors (DV2419-447, NITD449 and Doxycycline) and 43,465 compounds compiled from naturally derived product libraries comprising AfroDb, NANPDB and TCMID were screened against the envelope protein's energy-minimized structure as an integrated library. After the molecular docking studies involving 7200 prefiltered compounds and three known inhibitors using AutoDock Vina, 620 top-identified hits were physiochemically and pharmacologically profiled using SwissADME. Compared with reported potent inhibitors, the lead compounds were shown to have better binding affinities greater than −8.6 kcal/mol. Four predicted lead compounds comprising ZINC000014721518, ZINC000005195832, ZINC000014819293 and ZINC000004102396 were identified to interact with Thr48, Leu198 and Gln49, which are critical residues in the inhibition of membrane fusion. All the potential leads were predicted to be antiviral and membrane permeability inhibitors with Pa > 0.300 and Pa > 0.500, respectively. ZINC000014756860, ZINC000014819293 and ZINC000003871358 were predicted to be viral entry inhibitors. Structurally similar compounds have been shown to inhibit Dengue virus (DENV) replication. In-depth molecular dynamics simulations, including MM/PBSA computations, further substantiated the protein–ligand complexes' stability and favorable binding mechanisms with residues Leu198, Ile270, Thr48 and Phe193. Further experimental evaluation is needed to understand their role in inhibiting DENV viral entry.

KEYWORDS: Drug discovery; envelope protein; virtual screening; molecular dynamics; MM/PBSA.

Received: 1 August 2024
Accepted: 3 October 2024
Published: 9 January 2025

OPEN ACCESS
DOI: 10.1142/S2737416524500704

1. INTRODUCTION

Dengue virus (DENV) is a member of the Flaviviridae family and is responsible for the most prevalent mosquito-borne viral hemorrhagic fever.[1] The transmission of DENV to humans primarily occurs through mosquito bites from species such as *Aedes aegypti* and *Aedes albopictus*, which are widespread in tropical and subtropical climates, including both urban and rural regions.[2,3] The severe and sometimes fatal diseases known as dengue hemorrhagic fever (DHF) and dengue shock syndrome (DSS) can develop in certain people infected with DENV.[4] A total of 390 million worldwide DENV infections occur each year, of which 96 million have clinical symptoms.[5,6] The most severely affected regions include the Americas, Southeast Asia and the Western Pacific. In 2016, significant global outbreaks resulted in over 2.3 million reported cases in the Americas alone.[7] Furthermore, in 2018, during the Ebola virus disease (EVD) outbreak in Africa, two distinct DENV serotypes (DENV2 and DENV3) were identified in four out of 150 patients initially presumed to have Ebola virus disease.[8]

Despite considerable efforts, no clinically approved antiviral therapy for treating DENV infection exists. Patients afflicted with DENV typically receive symptomatic treatment and supportive care in a hospital setting.[9] The incidence of severe disease in the form of DHF and DSS is most likely to happen during secondary infections with another DENV serotype as a result of antibody-dependent enhancement (ADE) or original antigenic sin.[10,11] Given these challenges, there is a critical need to develop novel anti-dengue drugs. Numerous inhibitory agents have been explored for combating flaviviruses, targeting various cellular and viral components. These approaches include suppression of virion secretion and infectivity, assembly and maturation, monoclonal antibodies,[12] RNA silencing, peptides targeting the E protein and host cell receptor binding.[13] Additionally, rational design strategies have been employed to create compounds to disrupt the envelope protein's structural alterations during viral fusion.[3,14] However, despite these promising avenues, none of these known inhibitors have received approval for use as drugs.[5,10]

Its enveloped structure characterizes the DENV and possesses a single-stranded positive-sense RNA genome.[15,16] After being translated into a single polyprotein, the genomic RNA is cleaved by both host and viral proteases.[17] This cleavage process results in the formation of three structural proteins that collectively encapsulate the RNA genome. These proteins are capsid (C), membrane (M) and envelope (E). Additionally, the DENV genome encodes seven nonstructural proteins (NS1, NS2A, NS2B, NS3, NS4A, NS4B and NS5).[18] The pre-membrane (prM) protein plays a vital role in maintaining the spatial structure of the envelope protein.[19] Notably, the nonstructural proteins of DENV play regulatory roles in several phases of the virus's lifecycle, including RNA replication, the assembly of virions, the cleavage of the polyprotein, maturation processes and the defense mechanisms against host immunity.[20–22] Through receptor binding, receptor-mediated endocytosis, pH-mediated fusion and flaviviruses can infiltrate the host cells. This low pH-induced fusion releases viral genomic RNA into the cytoplasm of the host cell, starting the virus's replication cycle.[23,24]

The fusing of the viral and endosomal membranes, which releases the viral genome into the cytoplasm of the host cell, is caused by acidic endosomes stimulating the conformational rearrangement of viral E proteins.[25–27] The virion E protein is pivotal in orchestrating this initial entry process. It interacts with host cell receptors and promotes the fusion of the membranes of the virus and the host cell.[28] The Dengue DENV E protein's crystallographic study demonstrates the existence of a hydrophobic pocket between DI and DII of the structure normally occupied by the detergent *n*-octyl-β-D-glucoside (β-OG).[29,30] This hydrophobic pocket is critical in the conformational rearrangements necessary for membrane fusion under low-pH conditions.[31] As a result, the β-OG binding site has been recognized as a potential target for the development of small-molecule inhibitors that will interfere with the fusion process of the virus and host membrane.[31,32]

The structural information available for the DENV presented an opportunity to discover potent antiviral agents capable of disrupting the early stages of DENV infection. This study utilizes bioinformatics approaches targeting the hydrophobic binding site of β-OG within the envelope protein (PDB code: 1OKE) to predict new lead compounds to inhibit the activities of the envelope protein. Docking-based virtual screening was performed using naturally-derived products from three repositories comprising AfroDb,[33] Northern African Natural Product Database (NANP Db)[34] and traditional Chinese medicine integrative database (TCMID),[35] as well as known inhibitors as controls. The screening procedure commenced with an ADME filter to identify potentially nontoxic molecules suitable for drug development. Compounds

DOI: 10.1142/S2737416524500704

exhibiting high binding affinity following molecular docking were further subjected to pharmacological and physicochemical profiling to identify drug-like compounds among the candidates. Subsequently, the interactions and stabilities of the complexes were analyzed through protein–ligand interaction profiles and molecular dynamics simulations, respectively. To further explore the binding affinities, MM/PBSA calculations were performed. These calculations provided quantitative data on the complexes' binding energies, aiding in identifying potential inhibitory compounds.

2. MATERIALS AND METHODS

A graphical representation of the methodology applied to this study is presented (Fig. 1). The input and output files of the work have been provided as Supplementary File 1.

2.1. Selection of target and compounds

Structure-based approaches utilize a known three-dimensional (3D) structure obtained from techniques including as X-ray crystallography and nuclear magnetic resonance spectroscopy. The pre-fusion structure (dimeric form) of DENV2 was selected as the model for computational methods to identify potential viral entry inhibitors, after considering the resolution, *R* values and number of missing residues. The structure was obtained from the Protein Data Bank (PDB ID: 1OKE), at a resolution of 2.40 Å using X-ray diffraction. To perform molecular docking and identify potential entry inhibitors, an integrated compound library comprising a total of 43,465 compounds was sourced from naturally derived products, including databases such as AfroDb, the Northern African Natural Product Database (NANP DB) and the Traditional Chinese Medicine Integrative Database (TCMID). 832 and 37,707 compounds were obtained from AfroDb and TCMID, respectively, both catalogs of the ZINC15[36] database. Furthermore, 4924 compounds were obtained from NANPDB, an index of chemicals mostly derived from different sources, such as mammals, fungi, bacteria, plants and endophytes.[34] Three known DENV2 inhibitors comprising of DV2419-447, Doxycycline with IC_{50}s of 0.125 μM[13] and 55.6 μM,[37] respectively, and NITD449 with EC_{50} of 5 μM[38] were used as standards.

2.2. Prefiltering of library

The screening process commenced with applying an ADME filter, designed to retain compounds that exhibited the potential for being both nontoxic and suitable for drug development.[39,40] It was done based on a stringent filter that included five properties: Total average molecular weight (MW) in g/mol, the number of hydrogen bond donors, the number of hydrogen bond acceptors, the count of rotatable bonds and the partition coefficient, collectively known as Lipinski's Rule of Five.[41] A lead compound usually adheres to specific criteria, including a MW of around 500 Da, the ability to form hydrogen bonds

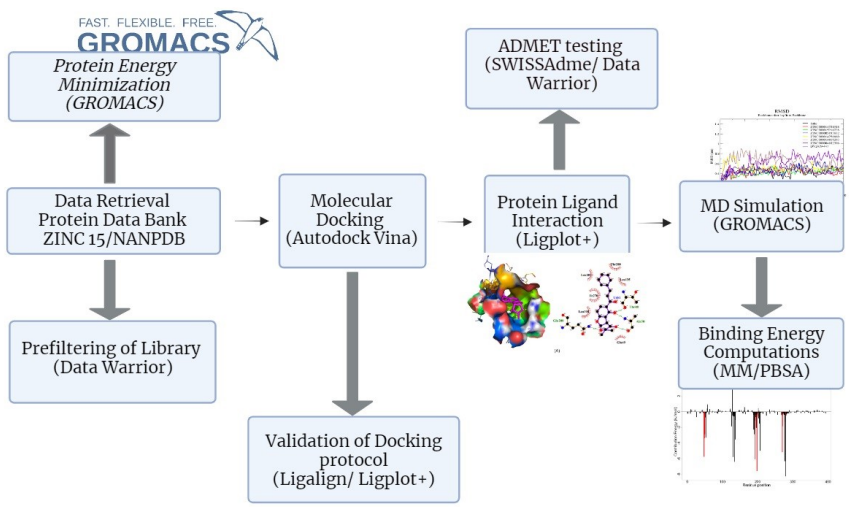

Fig. 1. (Color online) Graphical depiction of the methods and instruments utilized in this study's workflow.

DOI: 10.1142/S2737416524500704
J. Comput. Biophys. Chem. **2025**, *24* (5), 535–556

with its target (with no more than five hydrogen bond donors and no more than 10 hydrogen bond acceptors), flexibility characterized by a suitable number of rotatable bonds to enable effective binding and favorable lipophilicity as indicated by a partition coefficient (cLogP, a compound's lipophilicity affects its absorption into the body) of less than five.[42] OSIRIS DataWarrior (V5.2.1)[43] was used to eliminate ligands that violated these parameters.

2.3. Docking protocol validation

2.3.1. *Co-crystallized with re-docked complexes superimposition*

The detergent *n*-octyl-*β*-D-glucoside (*β*-OG) in the hydrophobic pocket at the hinge region between domains I and II was extracted from the co-crystalized structure of the envelope protein and re-docked into the same pocket using AutoDock Vina v0.8.[44] The predicted binding pose of the detergent *β*-OG was superimposed with the experimentally measured pose using LigAlign v1.0.[45] LigAlign is a software commonly employed for visualizing and interpreting ligand–protein interactions. The binding interactions at the active site were analyzed using LigPlot+ v1.4.5.[46]

2.3.2. *ROC curve analysis*

Using six recognized active compounds that specifically target the envelope protein, 300 decoys were produced using the Database of Useful Decoys (DUD-E).[47,48] Fifty decoys were generated for each active, designed to mimic the physiochemical properties of the active compounds. The actives and decoys were converted to AutoDock pdbqt format for molecular docking using AutoDock Vina to generate the ROC and Area under the curve (AUC). The curves were generated using easyROC v1.3[49] to assess the performance of molecular docking in distinguishing between the active compounds and the decoys. The AUC value, which ranges from zero to one, was calculated from the ROC curves. The AUC provides a quantitative measure of the model's ability to distinguish the active compounds from the decoys, with higher AUC values indicating better performance in distinguishing them apart.

2.4. Molecular docking of libraries and inhibitors

To identify potential inhibitors targeting the envelope protein, molecular docking experiments were executed using AutoDock Vina.[44] The active site for docking was the hydrophobic pocket of the protein. The filtered library of compounds and the inhibitors were converted to .pdbqt, and their energies were minimized using default parameters comprising Universal Force Field (UFF) and conjugate gradients for an optimization technique consisting of 200 steps to refine the energy of the compounds. Additionally, a set of inhibitors, including those currently in clinical trials, were included in the library. The dimension of the grid box was specified as follows: Center_x = −9.9335 Å center_y = 79.8626 Å center_z = 45.9350 Å size_x = 19.5764 Å size_y = 16.5928 Å size_z = 13.9531 Å. The screened compounds were ranked based on their binding affinities to the target, and possible poses were visually assessed using PyMOL 2.3.3.[50]

2.5. Protein–ligand interaction

Detailed analysis of the interactions between the critical residues within the active site and the selected compounds was conducted using LigPlot+ v1.4.5.[46] This analysis aimed to uncover and characterize various intermolecular interactions, including hydrophobic and hydrogen bonding interactions, critical in binding the compounds to the target protein's active site.

2.6. ADMET screening of the hits

After virtual screening, compounds with high binding energy were subjected to physiochemical profiling to assess their drug-likeness and water solubility. Simplified Molecular-Input Line-Entry System (SMILES) formats were created from the chemical structures. SwissAdme was used for the analysis of the pharmacokinetic characteristics of the predicted compounds[51] and OSIRIS DataWarrior V5.2.1. These tools provided insights into the compounds' key pharmacological attributes and physicochemical characteristics, including gastrointestinal (GI) absorption, solubility, Ames toxicity and hERG1 inhibitor potential. The aim was to eliminate potential weak drug candidates after evaluating binding interactions.[52] Additionally, the toxicity profiles were assessed using OSIRIS Property Explorer within DataWarrior, which predicts the likelihood of mutagenicity, tumorigenicity, irritancy and reproductive effects. Only compounds exhibiting drug-like characteristics were taken into consideration for additional examination.

DOI: 10.1142/S2737416524500704

2.7. Estimation of biological activity of compounds and structural similarity search

The prediction of activity spectra of substances (PASS) was utilized in forecasting the probable pharmacological effects of selected substances. PASS is a machine learning-based tool that leverages both statistical analysis and structural information to predict biological activities.[53,54] It predicts more than 300 pharmacological effects and biochemical mechanisms by analyzing the SMILES files. Predictions aid in identifying and prioritizing promising compounds for further investigation by providing valuable insights into their potential biological activities. Additionally, using DrugBank, a similarity search of the chosen compounds was carried out to find structural analogs displaying relevant biological activity.[55,56]

2.8. Molecular dynamics simulation

All molecular dynamics (MD) studies were performed for 100 ns using Gromacs-2018 (Groningen Machine for Chemical Simulations)[57,58] on a Dell EMC high-performance computing cluster located at the WACCBIP, University of Ghana, Accra, to investigate the system stability. MD was carried out for the unbound protein and complexes. The protein structure obtained from the PDB was initially visualized with PyMOL (PyMOL Molecular Graphics System, Version 2.3.3, Schrödinger, LLC) and pre-processed by removing crystal water molecules and verified that all the necessary atoms or residues were present in the system. Hydrogen atoms were modeled into the structure using the pdb2gmx before solvation. To neutralize the system, solvent molecules were swapped out for counter ions within a cubic cage that extended one nanometer past any protein atom.

The energy minimization of the protein was performed using the optimized potentials for liquid simulations (OPLS)/all atom (AA) force field until stability was achieved. Equilibration steps were followed, including temperature standardization to 300 K and pressure application to reach a density of 1000 kg/m^3. For the protein–ligand complexes, similar procedures were employed with some differences. The GROMOS96 43a1 force field was used, and ligand topology was generated using PRODRG with specific settings: Chirality: No, Charges: Full, EM: Yes. Trajectory analysis was carried out using various modules in GROMACS, including "gmx rms" for root mean square deviation, "gmx rmsf" for root mean square fluctuation, and "gmx gyrate" for the radius of gyration. All generated graphs and plots were visualized using Xmgrace.[59]

2.9. Binding energy computations using the MM/PBSA method

Molecular mechanics Poisson–Boltzmann surface area (MM/PBSA)[60] method was employed to predict the binding-free energy using the g_mmpbsa tool. Contributing terms to the binding-free energy, such as the van der Waals energies, electrostatic, electrostatic energy and polar and nonpolar solvation energy were evaluated.[57] Estimates were also made of the energy contributions made by each residue to the binding. The negative and positive values indicate favorable and unfavorable contributions, respectively. The MM/PBSA computations were graphed using the R programming software.

3. RESULTS AND DISCUSSION

3.1. Protein structure and binding site analysis

To select an appropriate 3D structure of DENV2 envelope protein for this study, a search conducted through the Protein databank yielded several structures with PDB IDs such as 1OKE, 4UT6, 10AN, 4UTC and differing resolutions of 2.40 Å, 3.20 Å, 2.75 Å and 3.08 Å, respectively. Resolution and *R*-values[61–63] were the primary criteria for selecting the structure, with PDB ID 1OKE being chosen. This structure comprises 394 amino acids in its A and B chains. The E glycoprotein adopts a polygonal shape in its mature virion form, with dimers forming polygons that cover the surface of the viral particle.[64] The central domain I include the amino terminus and features two disulfide bridges. The fusion peptide is included in domain II, an extended finger-like domain that aids in stabilizing the dimer.[65,66] This area is abundant in glycine and features three disulfide bridges.[19] A binding pocket exists between domains I and II, capable of interacting with hydrophobic ligands[67] (Fig. 2(a)). Due to its ability to interact with various cellular molecules, the E glycoprotein is an ideal target for developing antiviral agents.[28]

At the entrance of the β-OG pocket, specific amino acid residues with hydrophilic properties, including Thr48, Glu49, Gln200, Gln271, Ala50 and Thr280, with the potential to establish electrostatically favorable interactions with ligands are present. In recent

DOI: 10.1142/S2737416524500704
J. Comput. Biophys. Chem. **2025**, *24* (5), 535–556

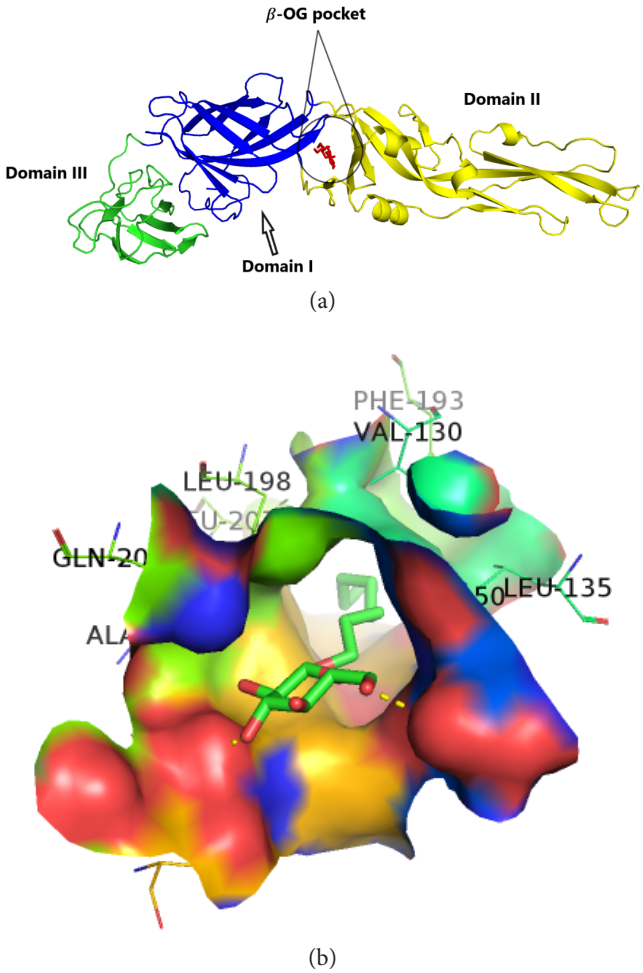

Fig. 2. (Color online) The structure of 1OKE. (a) Cartoon representation of 1OKE in complex with N-octyl-β-D-glucoside (β-OG) ligand. (b) β-OG molecule in the hydrophobic binding pocket of 1OKE protein. The binding site is depicted as surface and the β-OG molecule as stick. The image was generated using PyMOL.

investigations, docked ligands have been shown to form advantageous hydrogen bond interactions with Gln49, Ala50 and Gln200, even though none of these residues forms a hydrogen bond interaction with the β-OG ligand in the previously reported X-ray structure. However, several hydrophobic interactions have been reported between ligands and residues Gln271, Thr280, Leu277, Ile270, Phe193 and Leu207. The binding pocket and critical residues interacting with the β-OG ligand were visualized and analyzed using PyMOL version 2.3.3 (Fig. 2(b)).

3.2. Prefiltering of library

One of the significant reasons for drug failures is safety concerns. Therefore, it was crucial to identify molecules with suitable characteristics to ensure their safety as drugs. Out of 43,465 compounds obtained from the three databases, a total of 7200 obeyed Lipinski's rule of five: Molecules with a maximum of 10 hydrogen-bond-accepting atoms and a maximum of five hydrogen-bond-donating atoms, a MW of 500 g/mol or less, and a cLogP of five or less. Compounds meeting these criteria are often called "drug-like" because most clinically marketed drugs have MWs below 350 and cLogP values below three.[51,68] Solubility and permeability are also crucial when considering a compound's potential as a drug. This evaluation helps determine whether a compound can enter a patient's circulation through injection or absorption in the digestive system. Unfortunately, many molecules were disqualified due to their high MWs.

3.3. Docking protocol validation

3.3.1. *Superimposition of co-crystallized with re-docked complexes*

Prior to molecular docking, the docking accuracy of AutoDock Vina v0.8 was evaluated by docking the β-OG into the binding site of the envelope protein. First, the co-crystallized β-OG was removed using PyMOL and re-docked into the hydrophobic pocket using a grid box large enough to accommodate the β-OG molecule. To determine whether the co-crystal complex and the re-docked ligand complex exhibited similar binding interactions with critical residues, LigPlot+ v1.4.5 was employed to superimpose both complexes. This analysis revealed that eight critical residues had overlapping hydrophobic bond interactions. These residues included Thr48, Gln49, Ala50, Phe193, Leu207, Ile270, Gln271 and Thr280. This result demonstrates that AutoDock Vina was able to replicate a comparable position in the virtual screening environment.

Furthermore, the two complexes were aligned to validate molecular docking, yielding a root mean square deviation (RMSD) value of 1.071 Å. This value reaffirms the reliability of AutoDock Vina's docking accuracy. The overlapped residues revealed by LigPlot+ and the pose generated from the superimposition can be observed in Figs. 3 and 4, respectively.

3.3.2. *ROC curve analysis for the validation of the docking methodology*

The receiver operating curve (ROC) measures the docking software's accuracy and ability to effectively

DOI: 10.1142/S2737416524500704

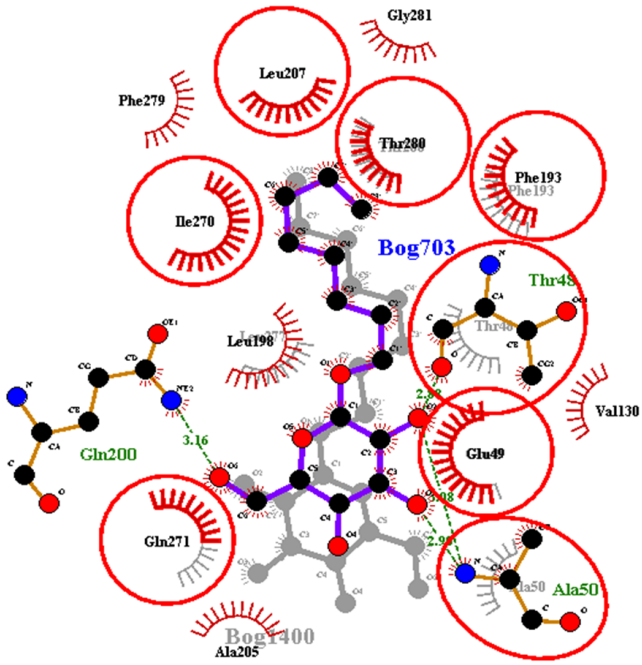

Fig. 3. (Color online) Superimposed LigPlots comparing the re-docked β-OG ligand and 1OKE. The red-circled residues signify the overlapping contacts between the re-docked complex and the co-crystallized ligand (β-OG).

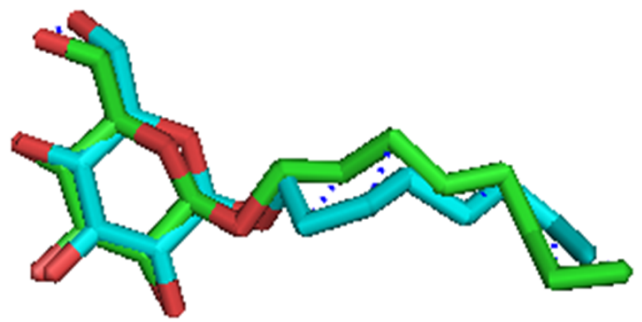

Fig. 4. (Color online) The cartoon representation of the superimposition of the co-crystallized β-OG ligand (green) and the re-docked β-OG ligand.

differentiate between docked active compounds and inactive (decoy) compounds for a specific target.[69] The area under the curve (AUC) of the ROC was generated using easyROC[70] upon completion of the docking. An AUC value close to one signifies a higher capability of the model to accurately identify between actives and decoys, while an AUC value closer to zero suggests a poorer ability to make this distinction. An AUC of one indicates perfect classification, while zero implies no classification capability. In the generated ROC curve (Fig. 5), the calculated AUC was found to be 0.73122, considered acceptable. This indicates that the docking

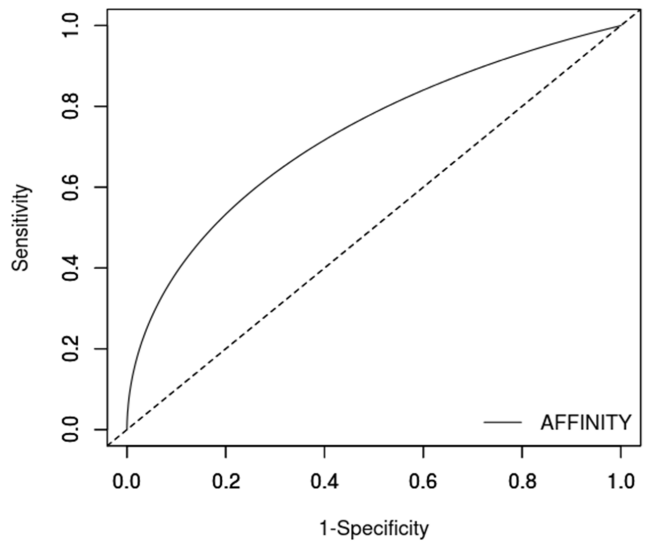

Fig. 5. An ROC curve generated by screening inhibitors with corresponding decoys against the β-OG binding pocket of the envelope protein. The AUC is 0.73122, which is in the acceptable range.

software demonstrates a reasonably good ability to differentiate between active and decoy compounds for the specific target under investigation. AUC values near one indicate that the model can more accurately identify between actives and decoys.

3.4. Molecular docking

Discovering a hit compound against a target is the process of molecular docking. It is mainly used in structure-based drug discovery because it enables the prediction of how ligands will fit into a target protein with a high degree of accuracy. A grid box measuring 19.5764 Å × 16.5928 Å × 13.9531 Å was used to screen 7200 prefiltered compounds and three inhibitors against the target, with center_x = −9.9335 Å, center_y = 79.8626 Å and center_z = 45.9350 Å. After using AutoDock Vina to screen those compounds successfully, ZINC000085550149 showed the highest binding energy toward the β-OG pocket among all ligands with an energy of −10.40 kcal/mol. The inhibitors, DV2419-447, NITD449 and Doxycycline, had binding energies of −7.7 kcal/mol, −6.5 kcal/mol and −5.1 kcal/mol, respectively. The compounds that exhibited binding energies of −8.0 kcal/mol or below were chosen using the inhibitors as reference points. The more negative binding energy, the stronger the bond between the target protein and the ligand. Binding energy estimates for 848 compounds were less than or equal to −8.0 kcal/mol. Upon visualizing the ligands' poses within the active site, it was

DOI: 10.1142/S2737416524500704
J. Comput. Biophys. Chem. **2025**, *24* (5), 535–556

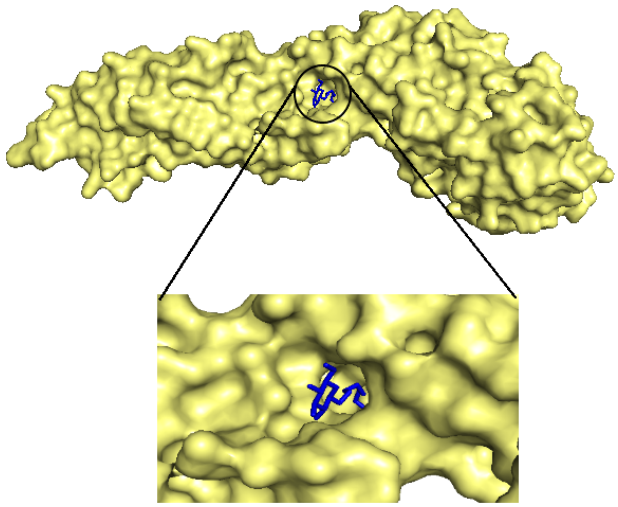

Fig. 6. (Color online) The ZINC000014721518 docked at the β-OG binding pocket of the envelope protein.

observed that 620 ligands docked securely and deeply in the active site, suggesting strong binding interactions. (Fig. 6). Compared to the known inhibitors utilized in the study, these compounds showed greater binding energies.

3.5. Protein–ligand interactions

The effect of favorable ligand interactions depend on the chemical features and bonds between the ligand and the target.[71] The interactions, specifically hydrogen and hydrophobic bonds, were thoroughly examined using LigPlot+ since they contribute significantly to stabilizing ligands within specific regions of a protein structure.[72] After analyzing the 620 shortlisted ligands, 26 of them showed strong interactions with at least two of the key amino acids, such as Gln200, Ala50, Thr280, Gln271 and Thr280, crucial for the membrane fusion process, which allows the viral genome to enter the cytoplasm of the infected cell. In terms of hydrogen bonding, ZINC000014756860 had the most hydrogen bonds of four, followed by ZINC000005195832, ZINC000014819293, ZINC000004102396, ZINC000014721518, ZINC000015216728, with three hydrogen bonds with critical residues. Similarly, cyclo-D-Trp-L-pro and ZINC000003871358 formed two strong hydrogen bond interactions. Finally, ZINC000040564501, ZINC000035941652 and ZINC000004102395 formed hydrogen bonds with only one amino acid. In previous studies, Doxycycline interacted with residues in the β-OG pocket, including Thr48, Glu49, Ala50, Gln271 and Gln200.[37] The molecular interaction of NITD449 and DV2419-447 after docking demonstrated hydrogen–bond interactions with Ala50, Gln200 and Gln271 (Table 1). Hydrophobic interaction and, most importantly, hydrogen bonds are crucial indicators of a stable complex. The compounds demonstrated stronger interactions with critical elements essential for pH-induced conformational

Table 1. The intermolecular bonds and binding energies between DENV2 and selected substances.

Predicted ligands	Binding energy (kcal/mol)	Hydrogen bonding	Hydrophobic bonding
ZINC000014756860	−8.6	Gln200, Ala50, Thr280, Gln271	Thr48, Gln49, Ile270, Leu207, Phe193, Leu198, Ala50
ZINC000005195832	−9.3	Gln200, Ala50, Gln271	Val130, Thr48, Gln49, Ile270, Phe279, Leu207, Phe193, Leu198, Ala205, Gly281, Thr280, Thr268
ZINC000014819293	−9.2	Gln200, Ala50, Gln271	Val130, Thr48, Gln49, Ile270, Phe279, Leu207, Phe193, Leu198, Ala205, Gly281, Thr280, Thr268
ZINC000004102396	−9.1	Gln200, Thr48, Gln271	Ile270, Leu277, Leu207, Phe193, Leu198, Ala205, Thr280, Thr268
ZINC000014721518	−9.0	Gln200, Ala50, Thr48	Gln49, Ile270, Leu207, Leu198, Thr280, Leu135
ZINC000015216728	−8.6	Gln200, Ala50, Gln271	Ala205, Gln49, Ile270, Leu207, Leu198, Phe193, Thr280, Thr48
ZINC000003871358	−8.6	Gln200, Ala50,	Thr280, Gln49, Ile270, Leu207, Leu198, Phe193, Ala205, Gln271, Thr48
cyclo-D-Trp-L-pro	−8.4	Ala50, Gln200	Gln271, Ala205, Thr48, Gln49, Leu198, Thr280, Ile270, Leu207
DV2419-447	−7.7	Gln271	Thr48, Gln49, Ala50, Gln200, Leu198, Thr280, Ile270, Leu207, Leu277, Lys47, Gly275, Phe193, Val130,
NITD449	−6.5	Ala50, Gln200, Gln271	Ala205, Thr48, Gln49, Leu198, Ile270, Leu277, Gln52, Lys128, Pro53
Doxycycline	−5.1	Ala50	Leu207, Thr48, Gln49, Gln200, Leu198, Thr280, Ile270, Leu277, Phe193, Val130, Ala205

DOI: 10.1142/S2737416524500704

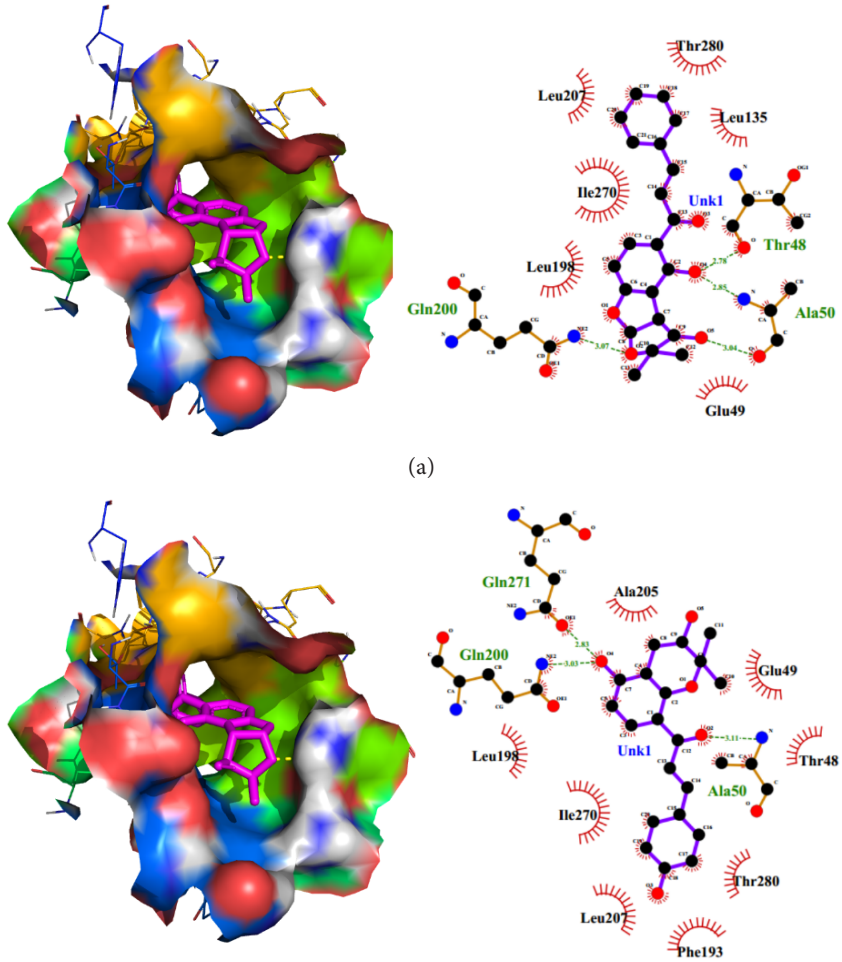

Fig. 7. (Color online) 2D and 3D representation of the protein–ligand interactions. (a) Visualization and interaction profiles of the 1OKE-ZINC000014721518 using Pymol and LigPlot+. (b) 1OKE-ZINC000015216728 complex shown using PyMOL and LigPlot+. For the 2D, hydrophobic interactions are represented by red spoke arcs, hydrogen bonds by green dashed lines and ligands by purple. For the 3D, the binding side is shown as surface and the β-OG molecule as stick.

changes required for DENV entry (Ala50, Gln200 and Gln271). Their LigPlots and PyMOL representations are depicted in Table 1 and Fig. 7.

3.6. *In silico* ADMET studies

The integrated library was prefiltered using DataWarrior based on Lipinski's rule and toxicity levels; however, other properties such as solubility, bioavailability, absorption and more were considered during the ADMET investigations, and based on Veber's. All 16 identified compounds passed due to their low total polar surface area (TPSA) values. High TPSA values indicate excellent human intestinal absorption (HIA) and Caco-2 permeability.[73] Moderate solubility was predicted for most compounds. OSIRIS DataWarrior (V5.2.1) was used to assess the toxicity of these compounds, and all 16 were predicted to be nonmutagenic, nontumorigenic and nonirritating. Pharmacokinetics properties comprised gastrointestinal (GI) absorption, cytochrome inhibition, P-glycoprotein (P-gp) substrates and blood–brain barrier (BBB) permeant of the predicted compounds, were also analyzed using SwissADME (Table 2).

Pharmacokinetics is crucial in determining how drugs are metabolized, distributed and eliminated in a living organism.[74] It was discovered that all the substances had high gastrointestinal absorption, suggesting a high chance of effective absorption into the bloodstream. Only ZINC000014721518 and ZINC000040564501 were predicted to have the potential to permeate the BBB, which determines the potential to traverse the brain.[75] A crucial aspect evaluated was the chemicals' potential to function as substrates for P-glycoprotein (P-gp), a protein involved in the

DOI: 10.1142/S2737416524500704
J. Comput. Biophys. Chem. **2025**, *24* (5), 535–556

Table 2. ADME prediction of the top 16 hits for TPSA, estimated solubility (ESOL) class, gastrointestinal absorption and MW.

Compounds	Molecular weight	GI absorption	ESOL log *S*	ESOL class	TPSA
ZINC000005195832	338.35	High	−5.33	Moderately soluble	90.9
cyclo-D-Trp-L-pro	283.33	High	−2.73	Soluble	65.2
ZINC000014819293	340.37	High	−4.91	Moderately soluble	86.99
ZINC000004102396	287.31	High	−1.86	Soluble	62.16
ZINC000014721518	352.38	High	−4.35	Moderately soluble	75.99
ZINC000014756860	300.26	High	−3.77	Soluble	100.13
ZINC000015216728	340.37	High	−3.98	Soluble	86.99
ZINC000003871358	284.26	High	−4.14	Moderately soluble	79.9
ZINC000035941652	300.26	High	−4.06	Moderately soluble	100.13
ZINC000040564501	334.45	High	−3.69	Soluble	74.6
ZINC000006483757	284.26	High	−4.08	Moderately soluble	79.9
ZINC000015115009	310.39	High	−5.12	Moderately soluble	49.69
ZINC000015147753	293.36	High	−4.45	Moderately soluble	38.33
ZINC000015115007	310.39	High	−5.12	Moderately soluble	49.69
ZINC000005543044	354.35	High	−3.72	Soluble	104.06
ZINC000014658084	356.37	High	−3.76	Soluble	66.38

elimination of medicines or foreign objects from the central nervous system (CNS). P-gp is involved in drug absorption, distribution and elimination.

3.7. Prediction of biological activity of shortlisted compounds and structural similarity search

Quantitative structure–activity relationship (QSAR), structure-based methods and machine learning algorithms are a few methods used to exploit the properties of biologically active substances. These properties of the active substances can be used to evaluate the toxicity or efficacy of the substances. Thus, the Prediction of Activity Spectra of Substances (PASS) [available at http://www.way2drug.com/passonline/] was used to investigate the biological activity of the selected promising compounds. The predicted activity is predominately based on the comparison of the structural nature of the submitted substance (SMILES) to a known entity in the database.[54] The activity is evaluated in terms of probable activity (Pa) and probable inactivity (Pi). The Pa is the probability of the compound to be active and Pi connotes the probability of the compound to be inactive. PASS predicts Pa and Pi for a given compound, ranging between zero and one for a predicted activity. Only compounds with a Pa value greater than Pi were considered for a specific pharmacological activity.[76]

With Pa>Pi, nine of the 16 hits were predicted to be antiviral. With Pa values of 0.307 and 0.322, respectively, and matching Pi values of 0.034 and 0.030, ZINC000014721518 and ZINC000015216728 were shown to have antiviral qualities. With Pa values of 0.393, 0.306, 0.334, 0.327, 0.584 and 0.425 and Pi values of 0.098, 0.236, 0.186, 0.200, 0.008 and 0.067, respectively, the compounds ZINC000005195832, ZINC000014756860, ZINC000015216728, ZINC000014721518, ZINC000014819293 and ZINC000004102396 were predicted to be antivirals with anti-Rhinovirus activity (Table 3). With Pa values larger than 0.3 and greater than their corresponding Pi values, the compounds, ZINC000003871358 and ZINC000040564501, were also found to possess additional antiviral activity against the influenza virus, hepatitis B and herpes.

Additionally, it was expected that ZINC000014756860, ZINC000014819293, ZINC000003871358 and cyclo-D-Trp-L-pro would impede viral entry, with matching Pi values of 0.034, 0.096, 0.032 and 0.056 and Pa values of 0.250, 0.218, 0.252 and 0.235, respectively. In addition, the tendency to be membrane permeability inhibitors and cell adhesion molecule inhibitors was also considered. There is evidence that several molecules in mammalian cells may act as receptors for the virus, including 3-grabbing nonintegrin, a dendritic cell-specific intercellular molecule.[26,28] Compounds ZINC000015216728 (Pa: 0.573; Pi: 0.010),

ZINC000014756860 (Pa: 0.307; Pi: 0.082), ZINC000005195832 (Pa: 0.332; Pi: 0.063), ZINC000014721518 (Pa: 0.235; Pi: 0.208) and ZINC000003871358 (Pa: 0.326; Pi: 0.067) were predicted to be cell molecule adhesion inhibitors (Table 3). The virus binds to receptors on the plasma membrane of the host cell to begin the entry of DENV thus inhibiting cell attachment this crucial.[77] ZINC000004102396 and ZINC000040564501 were predicted to possess platelet adhesion inhibitors with Pa values of 0.454 and 0.323, corresponding Pi values of 0.108 and 0.239, respectively. These predictions support the potential antiviral characteristics, making them intriguing candidates for subsequent *in vitro* investigations. With the exception of ZINC000004102396, all six possible lead compounds were also expected to be inhibitors of membrane permeability with Pa>0.529. Interacting with the envelope protein and inducing these pharmacological effects like membrane permeability and cell adhesion can block viral entry as proposed by several authors.[78–80]

Table 3. Predicted biological activity of the six selected hit compounds using PASS.

Compounds	Pa	Pi	Pa>Pi	Predicted pharmacologic activity
ZINC000014721518	0.327	0.200	Yes	Antiviral (Rhinovirus)
	0.307	0.034	Yes	Antiviral
	0.304	0.088	Yes	Antiviral (Herpes)
	0.529	0.131	Yes	Membrane permeability inhibitor
	0.235	0.208	Yes	Cell adhesion molecule inhibitor
ZINC000015216728	0.573	0.010	Yes	Cell adhesion molecule inhibitor
	0.538	0.018	Yes	Antiviral (Influenza)
	0.374	0.047	Yes	Antiviral (Herpes)
	0.334	0.186	Yes	Antiviral (Rhinovirus)
	0.322	0.030	Yes	Antiviral
	0.696	0.040	Yes	Membrane permeability inhibitor
ZINC000014756860	0.308	0.236	Yes	Antiviral (Rhinovirus)
	0.446	0.019	Yes	Antiviral (Herpes)
	0.402	0.015	Yes	Antiviral (Hepatitis B)
	0.337	0.069	Yes	Antiviral (Influenza)
	0.307	0.082	Yes	Cell adhesion molecule inhibitor
	0.949	0.002	Yes	Membrane permeability inhibitor
ZINC000005195832	0.449	0.018	Yes	Antiviral (Herpes)
	0.393	0.098	Yes	Antiviral (Rhinovirus)
	0.369	0.057	Yes	Antiviral (Influenza)
	0.309	0.031	Yes	Antiviral (Hepatitis B)
	0.332	0.063	Yes	Cell adhesion molecule inhibitor
ZINC000014819293	0.366	0.020	Yes	Antiviral (Hepatitis B)
	0.624	0.011	Yes	Antiviral (Influenza)
	0.584	0.008	Yes	Antiviral (Rhinovirus)
	0.496	0.010	Yes	Antiviral (Herpes)
	0.634	0.069	Yes	Membrane permeability inhibitor
ZINC000003871358	0.452	0.018	Yes	Antiviral (Herpes)
	0.417	0.013	Yes	Antiviral (Hepatitis B)
	0.424	0.039	Yes	Antiviral (Influenza)
	0.345	0.168	Yes	Antiviral (Rhinovirus)
	0.937	0.003	Yes	Membrane permeability inhibitor
	0.252	0.032	Yes	Viral entry inhibitor

(*Continued*)

DOI: 10.1142/S2737416524500704
J. Comput. Biophys. Chem. **2025**, *24* (5), 535–556

Table 3. (*Continued*)

Compounds	Pa	Pi	Pa > Pi	Predicted pharmacologic activity
	0.326	0.067	Yes	Cell adhesion molecule inhibitor
ZINC000004102396	0.425	0.067	Yes	Antiviral (Rhinovirus)
	0.319	0.075	Yes	Antiviral (Adenovirus)
cyclo-D-Trp-L-pro	0.135	0.049	Yes	Antiviral (Hepatitis)
	0.110	0.046	Yes	Antiviral (Hepatitis C)
	0.235	0.056	Yes	Viral entry inhibitor
ZINC000040564501	0.285	0.253	Yes	Membrane permeability inhibitor
	0.323	0.239	Yes	Platelet adhesion inhibitor
	0.676	0.007	Yes	Antiviral (Influenza)
	0.375	0.121	Yes	Antiviral (Rhinovirus)
	0.270	0.114	Yes	Antiviral (Herpes)

A DrugBank structural similarity search was conducted for the possible lead compounds [55,56] to support the PASS predictions. The compounds ZINC000005195832 and ZINC000014756860 were structurally similar to flavonoids including Apigenin, Hispidulin, Kaempferol, Luteolin, Quercetin, Myricetin and Fisetin, which have been shown to possess various pharmacological effects including, anticancer, antioxidant and antiviral activities.[81,82] Quercetin and Baicalein have been shown in studies to exhibit significant dengue replication inhibition properties with IC_{50} of 212.1 and IC_{50} of 13.5 μg/mL, respectively.[83] Fisetin, with similarity scores of 0.716 and 0.731 to ZINC000005195832 and ZINC000014756860, respectively, has been reported to inhibit DENV2 NGC in an LLC/MK2 cell-based system with EC_{50} of 192.15 μM.[84] Naringenin, a naringin precursor with virucidal activity against DENV2 (IC_{50} = 52.64 μg/Ml)[85] showed a similarity score of 0.836 to lead compound ZINC000014819293. Doxycycline, which has been demonstrated in studies to have an inhibitory effect on DENV replication, was predicted to have a structural similarity score of 0.658 to ZINC000004102396.[37,86] Finally, Naringin shown to inhibit DENV2 NG at MOI 1 in VERO cells (47.9 μg/mL)[85] was predicted to have a similarity score of 0.638 to the lead compound ZINC000014721518.

3.8. Molecular dynamics simulations

Structural stability and dynamic patterns are known to be observed in the protein by performing Molecular Dynamics simulations.[87] Based on the binding energies, hydrogen bond interactions with critical residues Gln200, Thr48, Ala50 and Gln271, and their availability for purchase, six out of the 16 hits were chosen for downstream analysis. Molecular dynamics was performed on the unbound protein, six selected compounds and DV2419-447, which had the highest binding energy amongst the three inhibitors. The radius of gyration (Rg), root mean squared deviation (RMSD) and root mean squared fluctuations (RMSF) are the main metrics used to assess stability.[88–90]

3.8.1. *The root mean square deviation of the unbound protein and complexes*

The RMSD calculation is performed based on the reference structure of a given protein. It considers the displacement of backbone atoms relative to the reference structure.[91,92] The unbound protein showed an initial increase up to a 5 ns time scale (Fig. 8) with an RMSD of about 0.5 nm. After about 5 ns, the RMSD ranged from 0.4 nm to 0.6 nm until 40 ns, where it fluctuated until

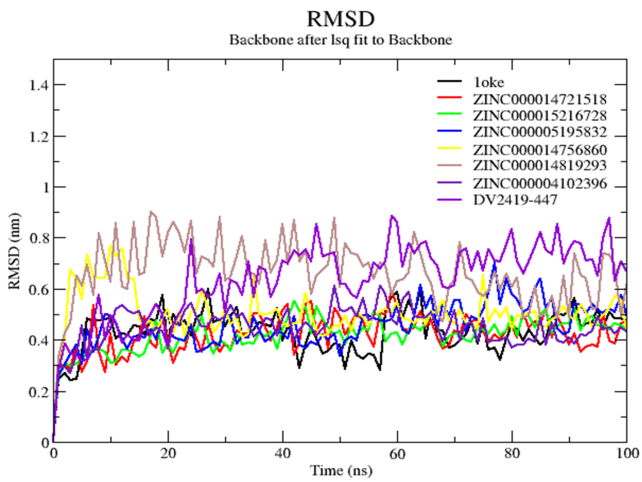

Fig. 8. (Color online) RMSD against time graph of the free protein and complexes.

DOI: 10.1142/S2737416524500704

80 ns, after which it remained relatively stable. This occurrence is quite the opposite for the protein–ligand complexes. 1OKE-ZINC000014721518 rose from 0.1 nm to 0.63 nm and showed relatively stable fluctuations till the 100 ns run. ZINC000015216728 showed the most stability throughout the simulation. It rose from 0.1 nm to 0.35 nm and achieved stability for the rest of the run, averaging 0.45 nm. ZINC000005195832 showed stable fluctuations after it rose to 0.45 nm with little deviations until 50 ns, where it deviated widely until 90 ns, where it became steady. The ZINC000014756860 complex endured significant fluctuations in the first 15 ns with an average RMSD of about 0.7 nm; however, it became reasonably stable for the remainder of the simulation. The protein-ZINC000014819293 was observed to be the least stable with very wide deviations, averaging 0.7 nm. It suggests that the binding of ZINC000014819293 may have caused conformational changes in the structure. The 1OKE-ZINC000004102396 complex showed stability after an initial rise to 0.43 nm at around 3 ns till 50 ns, with slight deviations, then maintained stability for the remainder of the run. In addition, the RMSD of the inhibitor DV2419-447 complexed with the protein had a sharp increase from 0 nm and peaked around 0.8 nm; it then oscillated widely between 0.5 nm and 0.8 nm (Fig. 8), with another peak at 85 ns averaging at 0.63 nm.

3.8.2. *Radius of gyration*

To further evaluate the stability of the complexes, the Rg was analyzed over a 100 ns simulation period. These Rg provide insights into the structural dynamics and compactness of the protein–ligand complexes, with lower and stable Rg values indicating more compact and stable complexes, while higher and fluctuating Rg values suggest less compact and potentially less stable complexes.[93] When a protein undergoes unfolding, its Rg would change over time. The Rg values of the unbound protein and all six complexes were between 3.0 nm and 3.6 nm (Fig. 9). The Rg of the protein demonstrated a steep rise from 0 ns to 8 ns, after which it experienced some fluctuations until 60 ns and again experienced a significant instability with an average of 3.5 nm. It remained relatively stable after the 60 ns till the end of the period. During the entire 100 ns simulation period, it was observed that the Rg values of all the complexes were consistently lower compared to that of the unbound protein. ZINC000014721518 and ZINC000015216728 complexes exhibited similar Rg trends. They experienced a gradual rise in Rg values until about 30 ns and maintained stability after a slight fall with an average of 3.35 nm. DV2419-447 complex had an average Rg of

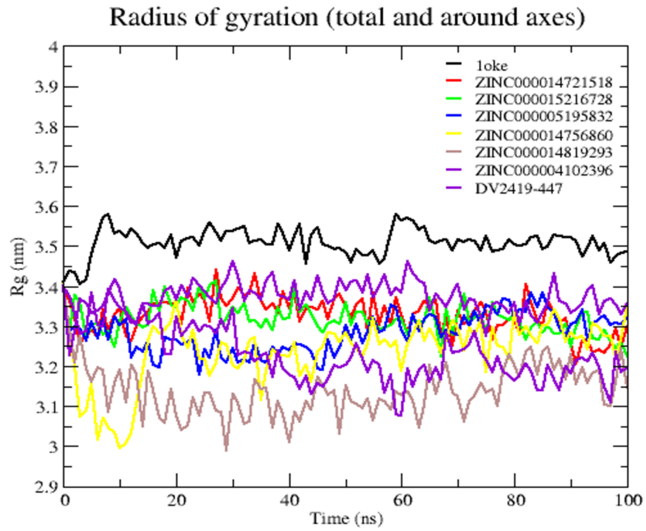

Fig. 9. (Color online) Radius of gyration against time graph of the complexes and the unbound protein.

approximately 3.25 nm. ZINC000005195832 complex experienced a decline from 0 ns to 10 ns, maintained a relatively steady Rg till 50 ns, and rose to 3.35 nm with an average. It finally showed little fluctuations till the end of the period. The opposite of this occurrence is seen in the 1OKE-ZINC000004102396. The Rg values for ZINC000014756860 and ZINC000014819293 showed various changes due to unstable Rg values.

3.8.3. *The root mean square fluctuations*

The RMSF analysis was conducted on both the unbound protein structure and the complexes to assess which residues contributed to structural fluctuations within the complexes.[94,95] Higher RMSF values indicate more significant fluctuations, often observed in protein regions associated with ligand binding and catalytic activity.[96] This analysis observed that all six compounds induced fluctuations in similar areas of the unbound 1OKE protein (Fig. 10). The compounds ZINC000014756860 and the inhibitor DV2419-449 exhibited the highest fluctuations, particularly in the regions spanning residue indices 40–90, 90–120 and 240–290. Residues ranging from 90 to 120 exhibited the highest fluctuations with values above 0.45 nm, suggesting possible structural changes resulting from the binding; however, the most increased fluctuations occurred between 90–120, and the molecular interactions failed to show any binding in that region. RMSD and gyrations graphs betoken some instability between 0 ns to 20 ns for ZINC000014756860. The RMSF corroborates the observation since it had the highest peak with a deviation from 0.21 nm to 1 nm.

DOI: 10.1142/S2737416524500704
J. Comput. Biophys. Chem. **2025**, *24* (5), 535–556

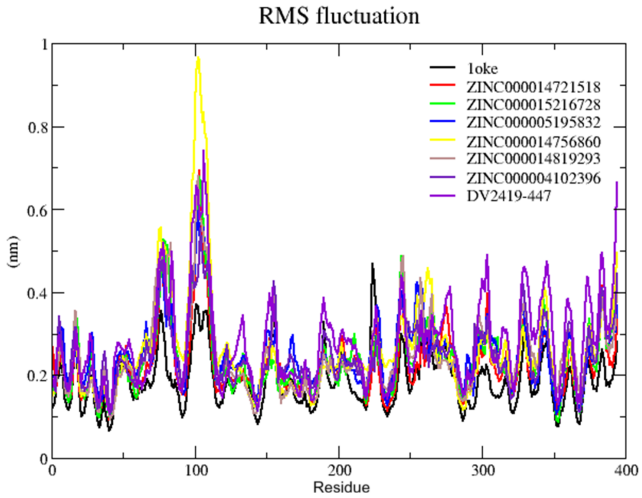

Fig. 10. (Color online) Estimation of RMSF trajectories of residues of the 1OKE-ligand complexes and unbound protein.

ZINC000014756860 was seen to exhibit hydrogen bonding with four critical residues. Intermittent fluctuations of the RMSD were observed in the DV2419-447 and 1OKE-ZINC000014819293 complex, indicating that during the simulated timescale, the other complexes and reference structures experienced just slight conformational changes and were hence more stable.

3.9. Evaluation of predicted leads using MM/PBSA computations

Molecular mechanics, combined with solvation models like Poisson–Boltzmann or generalized Born and surface area continuum solvation (MM/PBSA and MM/GBSA), are established methods for estimating the free binding energies when small molecular compounds interact with macromolecules.[97] The DV2419-447 inhibitor and the six predicted lead compounds' binding free energies were estimated using the Molecular Mechanics/Poisson–Boltzmann Surface Area (MM/PBSA) method. It quantifies the degree to which a ligand binds to its target, indicating the variation in free energy between the complexed and unbound states.[98] Thus, binding-free energy calculations are essential to understand better the binding conformations of lead compounds in drug discovery.[99] Furthermore, we assessed the contributions of various energy components, including electrostatic energy, polar and nonpolar solvation energy and van der Waals energy, to the overall binding energy,[60,100,101] as detailed in Table 4.

3.9.1. *MM/PBSA binding-free energy computations*

The results for the MM/PBSA revealed that the six predicted leads ZINC000014721518, ZINC000014819293, ZINC000015216728, ZINC000005195832, ZINC000004102396 and ZINC000014756860 had average binding-free energy of −210.116, −185.167, −164.321, −146.919, −87.326 and −42.984 kJ/mol, respectively (Table 4). In contrast, the inhibitor DV2419-447 showed a binding-free energy of −93.082 kJ/mol based on the MM/PBSA estimations (Table 4). ZINC000014721518 demonstrated the most negative Van der Waals energy with −242.218 kJ/mol, followed by ZINC000014819293 (−228.813), ZINC000015216728 (−198.505 kJ/mol) (Table 4). For SASA energy, the values were between −5.459 kJ/mol and −19.987 kJ/mol, with ZINC000014819293 and ZINC000014756860 demonstrating the most and least negative energy values, respectively. Though ZINC000015216728 had a higher binding energy of −8.6 kcal/mol from the docking results compared to the other leads, it was predicted to have a low-binding-free energy of −164.321 kJ/mol. The binding energy is mainly contributed by van der Waal energies and partly by electrostatic and

Table 4. Contributing energy terms for the 1OKE-ligand complexes in the MM/PBSA calculations. The average±standard deviations of energy data are displayed in kJ/mol.

Ligands	van der Waal energy (kJ/mol)	Electrostatic energy (kJ/mol)	Polar solvation energy (kJ/mol)	SASA energy (kJ/mol)	Binding energy (kJ/mol)
ZINC000014756860	−59.128±6.262	−17.583±2.267	39.015±5.271	−5.459±0.574	−42.984±4.279
ZINC000005195832	−194.493±1.688	−94.334±6.762	159.859±5.857	−17.953±0.100	−146.919±2.788
ZINC000004102396	−101.128±2.136	−110.249±5.692	132.727±5.508	−8.926±0.160	−87.326±4.120
ZINC000014721518	−242.218±1.804	−16.276±0.601	67.316±0.843	−18.974±0.101	−210.116±1.961
ZINC000014819293	−228.813±1.292	−20.674±0.515	84.389±1.080	−19.987±0.100	−185.167±1.466
ZINC000015216728	−198.505±24.810	−16.073±6.792	65.620±12.155	−15.363±1.512	−164.321±25.923
DV2419-447	−168.722±29.043	−86.724±22.787	177.806±33.305	−15.442±1.504	−93.082±32.570

Table 5. Predicted leads, along with their 2D structures and IUPAC designations, are sourced from the ZINC15 database.

Compound ID	IUPAC names	2D structure
ZINC000014756860	5,7-dihydroxy-2-(2-hydroxyphenyl)-6-methoxy-4H-chromen-4-one	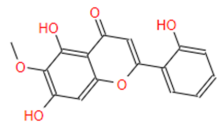
ZINC000005195832	5,7-dihydroxy-2-[4-hydroxy-3-(3-methylbut-2-en-1-yl) phenyl]-4H-chromen-4-one	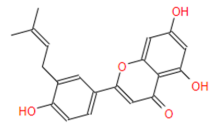
ZINC000004102396	(1S,13S,15S,16S)-5,7-dioxa-12-azapentacyclo[10.6.1.$0^{2,10}$.$0^{4,8}$.$0^{13,18}$] nonadeca-2,4(8),9,17-tetraene-15,16-diol	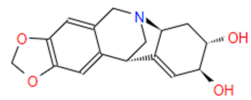
ZINC000014721518	(2E)-1-[(2S,3S,6R)-3,12-dihydroxy-4,4-dimethyl-5,7-dioxatricyclo[6.4.0.$0^{2,6}$]dodeca-1(12),8,10-trien-11-yl]-3-phenylprop-2-en-1-one	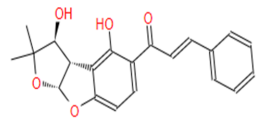
ZINC000014819293	(2R)-5,7-dihydroxy-2-[4-hydroxy-3-(3-methylbut-2-en-1-yl) phenyl]-3,4-dihydro-2H-1-benzopyran-4-one	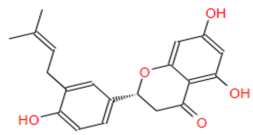
ZINC000015216728	(2E)-1-[(3S)-3,5-dihydroxy-2,2-dimethyl-3,4-dihydro-2H-1-benzopyran-8-yl]-3-(4-hydroxyphenyl)prop-2-en-1-one	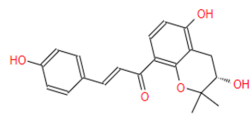

nonpolar solvation energies (Table 4). ZINC000014756860, which had the same binding energy as ZINC000015216728 (−8.6 kcal/mol), was predicted to possess the highest binding-free energy of −42.984 kJ/mol. The relatively low binding-free energies of these leads make them promising anti-dengue molecules. Results from docking and molecular interactions agree with the binding-free energy. A summary of the predicted leads is displayed in Table 5.

3.9.2. *Per-residue energy decomposition*

The per-residue energy decompositions were conducted to estimate further the individual energetic contributions of each residue (Fig. 11 and Supplementary Figures 1A–1F). This analysis offers valuable insights into the significant interactions involving key residues.[102,103] Notable residues that contribute energy above 5 kJ/mol or below −5 kJ/mol should be taken into account as being essential for the binding of a chemical to a protein.[98] Previous studies have demonstrated that amino acid residues such as Thr48, Gln49, Ala50, Phe193, Phe198 Gln200 and Ile270 in the β-OG binding site are fundamental in the inhibition of membrane fusion as thus were considered in these calculations. For the 1OKE-ZINC000014721518 complex, Thr48, Phe193, Leu198 and Ile270 contributed energies above than ±5 kJ/mol threshold with energies of −5.7441 kJ/mol, −6.0647 kJ/mol, −7.5716 kJ/mol and −5.1710 kJ/mol, respectively (Fig. 11). Only Gln49 contributed

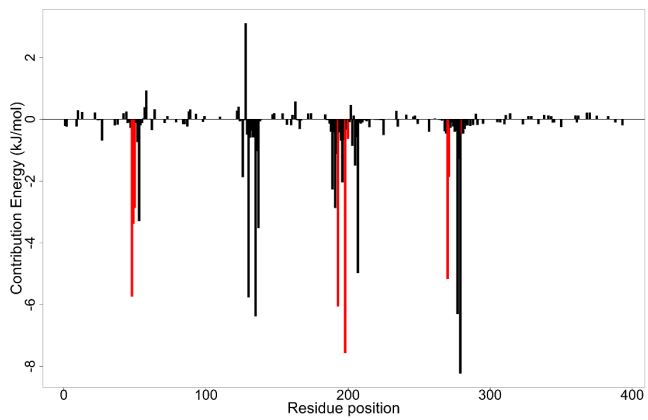

Fig. 11. (Color online) MM/PBSA plot for the 1OKE-ZINC000014721518 complex highlighting the energy contribution per residue with fluctuations indicated in red for critical residues.

DOI: 10.1142/S2737416524500704
J. Comput. Biophys. Chem. **2025**, *24* (5), 535–556

energy beyond the threshold of ±5 kJ/mol (−18.7259) in the 1OKE-ZINC000004102396 complex (Fig. S1(E)). For the inhibitor DV2419-447, Glu49 contributed above the threshold with an energy of 5.81 kJ/mol (Fig. S1(F)). Additionally, Leu198, Ile270, Thr48 and Phe193 contributed energies of −8.1278 kJ/mol, −5.6159 kJ/mol, −5.1915 kJ/mol and −7.7378 kJ/mol, respectively, in the 1OKE-ZINC000014819293 complex (Fig. S1(D)). For the 1OKE-ZINC000005195832 complex, Gln49 and Leu198 contributed 25.0377 and −11.1667, respectively.

4. CONCLUSION

Blocking the hydrophobic pocket or limiting hinge flexibility could hinder the membrane fusion process pocket.[104] African natural compounds such as ZINC000004102396, ZINC000014721518, ZINC000014819293, ZINC000015216728 and ZINC000005195832 were identified as novel potential lead compounds against the DENV E. These potential lead compounds satisfied the Lipinski's rule of 5 to support the physicochemical properties as druglike. By analyzing results obtained using the various computer-aided drug design techniques, the five compounds were predicted to have favorable pharmacological profiles with a high GI absorption indicating a high chance of absorption into the bloodstream with favorable binding energies and mechanisms. These findings support the hypothesis of an inhibitory mechanism involving ligand binding to the E protein pocket, potentially disrupting maturation or host-cell entry. Molecular dynamics and MM/PBSA computations were conducted to corroborate the findings obtained from the molecular docking and target–compound interactions and these formed the basis for identifying potential potent inhibitors against the DENV E protein. The results from the MM/PBSA showed that the compounds ZINC000004102396, ZINC000014721518, ZINC000014819293, ZINC000015216728, ZINC000005195832 and ZINC000014756860 had average binding free energies of −87.326, −210.116, −185.167, −164.321, −146.919 and −42.984 kJ/mol, respectively. All six plausible lead compounds also exhibited antiviral activity with a Pa > Pi alongside Pa above 0.3. They were also predicted as viral entry inhibitors, membrane permeable and structurally similar to compounds shown to have anti-DENV activity. These predicted compounds hold promise for further development into effective therapeutic moieties against the DENV and the findings can be corroborated experimentally to expedite the global quest for efficacious anti-dengue medications.

SUPPLEMENTARY MATERIAL

Supporting information document contains the plots for MM/PBSA binding-free energy contribution per residue of protein–ligand complexes, (A) 1oke-ZINC000015216728, (B) ZINC000005195832, (C) 1oke-ZINC000014756860, (D) 1oke-ZINC000014819293, (E) 1oke-ZINC000004102396 and (F) 1oke-DV2419-447. The Supplementary Information are available at: https://www.worldscientific.com/doi/suppl/10.1142/S2737416524500704.

ACKNOWLEDGMENTS

The authors are appreciative to the West African Centre for Cell Biology of Infectious Pathogens, University of Ghana, for permitting the use of Zuputo, their high-performance computer equipment. Professor Wilson died during the first revision of this paper. This work is dedicated to his memory and we are grateful for his mentorship and guidance of numerous students and researchers.

STATEMENT OF USAGE OF ARTIFICIAL INTELLIGENCE

None.

DATA AVAILABILITY

All data regarding this research are included in the paper and the supplementary materials.

AUTHORS' CONTRIBUTIONS

This project was primarily planned and designed by Samuel K. Kwofie, with assistance from George Hanson and Michael D. Wilson. The computational work was mostly done by George Hanson, Samuel K. Kwofie and Nana Effiansah Asmah, with assistance from Emmanuel Broni and Millicent Abena Adzagbo. This paper's first draft was written by George Hanson. This paper was edited and reviewed by Emmanuel Broni, Samuel K. Kwofie, Michael D. Wilson and Gifty Adobea Nyarko. Before submission, all writers approved the final paper.

CONFLICT OF INTEREST

The authors declare no conflict of interest.

FUNDING INFORMATION

This work was not funded.

ORCID

George Hanson
https://orcid.org/0009-0007-2720-9102
Nana Effiansah Asmah
https://orcid.org/0009-0006-6224-4918
Millicent Abena Adzagbo
https://orcid.org/0009-0008-6754-5562
Gifty Adobea Nyarko
https://orcid.org/0009-0006-8084-4933
Emmanuel Broni
https://orcid.org/0000-0002-6793-7530
Samuel K. Kwofie
https://orcid.org/0000-0002-1093-1517

References

1. Chao, L. H.; Jang, J.; Johnson, A.; Nguyen, A.; Gray, N. S.; Yang, P. L.; Harrison, S. C. How Small-Molecule Inhibitors of Dengue-Virus Infection Interfere with Viral Membrane Fusion. *Elife* **2018**, *7*, e36461.
2. Dang, M.; Lim, L.; Roy, A.; Song, J. Myricetin Allosterically Inhibits the Dengue NS2B-NS3 Protease by Disrupting the Active and Locking the Inactive Conformations. *ACS Omega* **2022**, *7* (3), 2798–2808, https://doi.org/10.1021/acsomega.1c05569.
3. Tariq, H.; Mumtaz, M.; Aslam, T.; Husnain, M.; Hussain, N.; Ali, M. Computational Approaches to Design Multi Epitope-Based Vaccine Designing of Dengue Virus -2 Enveloped Protein for Dengue Virus. *Pak. J. Health Sci.* **2024**, *5* (3), 55–61, https://doi.org/10.54393/pjhs.v5i03.1341.
4. Norshidah, H.; Leow, C. H.; Ezleen, K. E.; Wahab, H. A.; Vignesh, R.; Rasul, A.; Lai, N. S. Assessing the Potential of NS2B/NS3 Protease Inhibitors Biomarker in Curbing Dengue Virus Infections: *In Silico* vs. *In Vitro* Approach. *Front. Cell. Infect. Microbiol.* **2023**, *13* (February), 1–17, https://doi.org/10.3389/fcimb.2023.1061937.
5. Anasir, M. I.; Ramanathan, B. Structure-Based Design of Antivirals against Envelope Glycoprotein of Dengue Virus. *Viruses* **2020**, *12* (4), 367.
6. Rachmawati, Y.; Ekawardhani, S.; Fauziah, N.; Faridah, L.; Watanabe, K. Potential Way to Develop Dengue Virus Detection in Aedes Larvae as an Alternative for Dengue Active Surveillance: A Literature Review. *Trop. Med. Infect. Dis.* **2024**, *9* (3), 60, https://doi.org/10.3390/tropicalmed9030060.
7. Gebhard, L. G.; Leal, E. S.; Adler, N. S.; Fern, G. A.; Battini, L.; Aucar, M. G.; Videla, M.; Eugenia, M.; Ríos, D. L.; Alejandro, J.; Acosta, D.; Hern, A.; Cordo, S. M.; García, C. C.; Gamarnik, A. V; Cavasotto, C. N.; Bollini, M. De Novo Design Approaches Targeting an Envelope Protein Pocket to Identify Small Molecules against Dengue Virus. *Eur. J. Med. Chem.* **2019**, *182*, 111628, https://doi.org/10.1016/j.ejmech.2019.111628.
8. Humphrey, J.; Bonney, K.; Hayashi, T.; Dadzie, S.; Agbosu, E.; Pratt, D.; Nyarko, S.; Id, F. A.; Ido, E.; Sarkodie, B.; Ohta, N.; Yamaoka, S. Molecular Detection of Dengue Virus in Patients Suspected of Ebola Virus Disease in Ghana. *PLoS One* **2018**, *13* (12), e0208907.
9. Kok, W. M Expert Opinion on Drug Discovery New Developments in Flavivirus Drug Discovery New Developments in Flavivirus Drug Discovery. *Expert Opin. Drug Discov.* **2016**, *11* (5), 433–445, https://doi.org/10.1517/17460441.2016.1160887.
10. Lee, M. F.; Wu, Y. S.; Poh, C. L. Molecular Mechanisms of Antiviral Agents against Dengue Virus. *Viruses* **2023**, *15* (3), 705, https://doi.org/10.3390/v15030705.
11. M. Christopher, A. M. L. S. 乳鼠心肌提取 HHS Public Access. *Physiol. Behav.* **2016**, *176* (1), 100–106, https://doi.org/10.1160/TH09-03-0208.Plasma.
12. Rothan, H. A.; Han, H. C.; Ramasamy, T. S.; Othman, S.; Rahman, N. A.; Yusof, R. Inhibition of Dengue NS2B-NS3 Protease and Viral Replication in Vero Cells by Recombinant Retrocyclin-1. *BMC Infect. Dis.* **2012**, *12*, 314, https://doi.org/10.1186/1471-2334-12-314.
13. Chew, M. F.; Poh, K. S.; Poh, C. L. Peptides as Therapeutic Agents for Dengue Virus. *Int. J. Med. Sci.* **2017**, *14* (13), 1342–1359, https://doi.org/10.7150/ijms.21875.
14. Kampmann, T.; Yennamalli, R.; Campbell, P.; Stoermer, M. J.; Fairlie, D. P.; Kobe, B.; Young, P. R. *In Silico* Screening of Small Molecule Libraries Using the Dengue Virus Envelope E Protein Has Identified Compounds with Antiviral Activity against Multiple Flaviviruses. *Antiviral Res.* **2009**, *84* (3), 234–241, https://doi.org/10.1016/j.antiviral.2009.09.007.
15. Nanaware, N.; Banerjee, A.; Mullick Bagchi, S.; Bagchi, P.; Mukherjee, A. Dengue Virus Infection: A Tale of Viral Exploitations and Host Responses. *Viruses* **2021**, *13* (10), 1967, https://doi.org/10.3390/v13101967.
16. Boerneke, M. A.; Gokhale, N. S.; Horner, S. M.; Weeks, K. M. Structure-First Identification of RNA Elements That Regulate Dengue Virus Genome Architecture and Replication. *Proc. Natl. Acad. Sci. U. S. A.* **2023**, *120*

(15), e2217053120, https://doi.org/10.1073/pnas.2217053120.

17. Dwivedi, V. D.; Tripathi, I. P.; Tripathi, R. C.; Bharadwaj, S.; Mishra, S. K. Genomics, Proteomics and Evolution of Dengue Virus. *Brief. Funct. Genomics* **2017**, *16* (4), 217–227, https://doi.org/10.1093/bfgp/elw040.
18. Khalili, N. S. D.; Khawory, M. H.; Salin, N. H.; Zakaria, I. I.; Hariono, M.; Mikhaylov, A. A.; Kamarulzaman, E. E.; A Wahab, H.; Supratman, U.; Nurul Azmi, M. Synthesis and Biological Activity of Imidazole Phenazine Derivatives as Potential Inhibitors for NS2B-NS3 Dengue Protease. *Heliyon* **2024**, *10* (2), e24202, https://doi.org/10.1016/j.heliyon.2024.e24202.
19. Zhang, X.; Jia, R.; Shen, H.; Wang, M.; Yin, Z. Structures and Functions of the Envelope Glycoprotein in Flavivirus Infections. *Viruses* **2017**, *9* (11), 1–14, https://doi.org/10.3390/v9110338.
20. Bhargavi, S.; Reddy, G.; Chin, W.; Shivananju, N. S. Dengue Virus NS2 and NS4 : Minor Proteins, Mammoth Roles. *Biochem. Pharmacol.* **2018**, *154*, 54–63, https://doi.org/10.1016/j.bcp.2018.04.008.
21. Ramirez, R. R. Ludert, E. The Dengue Virus Nonstructural Protein 1 (NS1) Is Secreted from Mosquito Cells in Association with the Intracellular Cholesterol Transporter Chaperone Caveolin Complex. *J. Virol.* **2019**, *93* (4), 1–25. https://doi.org/https://doi.org/10.1128/jvi.01985-18.
22. Silva, E. M.; Conde, J. N.; Allonso, D.; Ventura, G. T.; Coelho, D. R.; Carneiro, P. H.; Silva, M. L.; Paes, M. V; Rabelo, K. Dengue Virus Nonstructural 3 Protein Interacts Directly with Human Glyceraldehyde-3-Phosphate Dehydrogenase (GAPDH) and Reduces Its Glycolytic Activity. *Sci. Rep*. **2019**, *9* (1), 1–19, https://doi.org/10.1038/s41598-019-39157-7.
23. Fishburn, A. T.; Pham, O. H.; Kenaston, M. W.; Beesabathuni, N. S.; Shah, P. S. Let's Get Physical: Flavivirus-Host Protein–Protein Interactions in Replication and Pathogenesis. *Front. Microbiol.* **2022**, *13* (March), 847588, https://doi.org/10.3389/fmicb.2022.847588.
24. Escalante, A. A.; Cepeda, A. S.; Pacheco, M. A. Why Plasmodium Vivax and Plasmodium Falciparum Are so Different ? A Tale of Two Clades and Their Species Diversities. *Malar. J.* **2022**, *21*, 1–19. https://doi.org/10.1186/s12936-022-04130-9.
25. Modis, Y.; Ogata, S.; Clements, D.; Harrison, S. C. Structure of the Dengue Virus Envelope Protein after Membrane Fusion. *Nature* **2004**, *427*, 313–319.
26. Schaar, H. M. Van Der; Rust, M. J.; Waarts, B.; Ende-metselaar, H. Van Der; Kuhn, R. J.; Wilschut, J.; Zhuang, X.; Smit, J. M. Characterization of the Early Events in Dengue Virus Cell Entry by Biochemical Assays and Single-Virus Tracking. *J. Virol.* **2007**, *81* (21), 12019–12028, https://doi.org/10.1128/JVI.00300-07.
27. Zhang, Y.; Zhang, W.; Ogata, S.; Clements, D.; Strauss, J. H.; Baker, T. S.; Kuhn, R. J.; Rossmann, M. G.; Street, W. S.; Lafayette, W. Conformational Changes of the Flavivirus E Glycoprotein. *Structure* **2004**, *12*, 1607–1618, https://doi.org/10.1016/j.str.2004.06.019.
28. Guardia, C. D. La; Lleonart, R. Progress in the Identification of Dengue Virus Entry/Fusion Inhibitors. *Biomed. Res. Int*. **2014**, *2014*, 825039.
29. Mir, A.; Ismatullah, H.; Rauf, S.; Niazi, U. H. K. Identification of Bioflavonoid as Fusion Inhibitor of Dengue Virus Using Molecular Docking Approach. *Inf. Med. Unlocked* **2016**, *3*, 1–6, https://doi.org/https://doi.org/10.1016/j.imu.2016.06.001.
30. Gallo, F. N.; Marquez, A. B.; Fidalgo, D. M.; Dana, A.; Dellarole, M.; García, C. C.; Bollini, M. Antiviral Drug Discovery: Pyrimidine Entry Inhibitors for Zika and Dengue Viruses. *Eur. J. Med. Chem.* **2024**, *272*, 116465, https://doi.org/10.1016/j.ejmech.2024.116465.
31. Leal, E. S.; Aucar, M. G.; Gebhard, L. G.; Iglesias, N. G.; Pascual, M. J.; Casal, J. J.; Gamarnik, A. V; Cavasotto, C. N.; Bollini, M. Discovery of Novel Dengue Virus Entry Inhibitors via a Structure-Based Approach. *Bioorg. Med. Chem. Lett.* **2017**, *27* (16), 3851–3855, https://doi.org/10.1016/j.bmcl.2017.06.049.
32. Liu, H. Y.; Yang, P. L. Small-Molecule Inhibition of Viral Fusion Glycoproteins. *Annu. Rev. Virol.* **2021**, *8* (1), 459–489, https://doi.org/10.1146/annurev-virology-022221-063725.
33. Ntie-kang, F.; Zofou, D.; Babiaka, S. B.; Meudom, R.; Scharfe, M.; Lifongo, L. L.; Mbah, J. A.; Meva, L.; Sippl, W.; Efange, S. M. N. AfroDb : A Select Highly Potent and Diverse Natural Product Library from African Medicinal Plants. *PLoS One* **2013**, *8* (10), e78085, https://doi.org/10.1371/journal.pone.0078085.
34. Ntie-kang, F.; Telukunta, K. K.; Do, K.; Simoben, C. V; Moumbock, F. A.; Malange, Y. I.; Njume, L. E.; Yong, J. N.; Sippl, W.; Gu, S. NANPDB: A Resource for Natural Products from Northern African Sources. *J. Nat. Prod.* **2017**, *80* (7), 2067–2076, https://doi.org/10.1021/acs.jnatprod.7b00283.
35. Chen, C. Y. TCM Database @ Taiwan: The World's Largest Traditional Chinese Medicine Database for Drug Screening *In Silico*. *PLoS One* **2011**, *6* (1), e15939, https://doi.org/10.1371/journal.pone.0015939.
36. Sterling, T.; Irwin, J. J. ZINC 15 - Ligand Discovery for Everyone. *J. Chem. Inf. Model.* **2015**, *55* (11), 2324–2337, https://doi.org/10.1021/acs.jcim.5b00559.
37. Yang, J. M.; Chen, Y. F.; Tu, Y. Y.; Yen, K. R.; Yang, Y. L. Combinatorial Computational Approaches to

Identify Tetracycline Derivatives as Flavivirus Inhibitors. *PLoS One* **2007**, *2* (5), 1–10, https://doi.org/10.1371/journal.pone.0000428.

38. Chen, Y. L.; Yin, Z.; Lakshminarayana, S. B.; Qing, M.; Schul, W.; Duraiswamy, J.; Kondreddi, R. R.; Goh, A.; Xu, H. Y.; Yip, A.; Liu, B.; Weaver, M.; Dartois, V.; Keller, T. H.; Shi, P. Y. Inhibition of Dengue Virus by an Ester Prodrug of an Adenosine Analog. *Antimicrob. Agents Chemother.* **2010**, *54* (8), 3255–3261, https://doi.org/10.1128/AAC.00397-10.
39. Martínez-Archundia, M.; Bello, M.; Correa-Basurto, J. Design of Drugs by Filtering Through ADMET, Physicochemical and Ligand-Target Flexibility Properties. *Methods Mol. Biol.* **2018**, *1824*, 403–416, https://doi.org/10.1007/978-1-4939-8630-9_24.
40. Guan, L.; Yang, H.; Cai, Y.; Sun, L.; Di, P.; Li, W.; Liu, G.; Tang, Y. ADMET-Score-a Comprehensive Scoring Function for Evaluation of Chemical Drug-Likeness. *MedChemComm* **2019**, *10* (1), 148–157, https://doi.org/10.1039/C8MD00472B.
41. Ditri, E. L. Z. and J. W. Screening The Efficacy of Melatonin on Neurodegeneration Mediated by ER Stress, Inflammation and Oxidative Damage. *Physiol. Behav.* **2017**, *176* (1), 139–148, https://doi.org/10.1016/j.addr.2016.05.007.BDDCS.
42. Hughes, J. P.; Rees, S. S.; Kalindjian, S. B.; Philpott, K. L. Principles of Early Drug Discovery. *Br. J. Pharmacol.* **2011**, *162* (6), 1239–1249, https://doi.org/10.1111/j.1476-5381.2010.01127.x.
43. Sander, T.; Freyss, J.; Von Korff, M.; Rufener, C. DataWarrior: An Open-Source Program for Chemistry Aware Data Visualization and Analysis. *J. Chem. Inf. Model.* **2015**, *55* (2), 460–473, https://doi.org/10.1021/ci500588j.
44. Trott, O.; Olson, A. J. AutoDock Vina: Improving the Speed and Accuracy of Docking with a New Scoring Function, Efficient Optimization, and Multithreading. *J. Comput. Chem.* **2010**, *31* (2), 455–461, https://doi.org/10.1002/jcc.21334.
45. Heifets, A.; Lilien, R. H. LigAlign: Flexible Ligand-Based Active Site Alignment and Analysis. *J. Mol. Graph. Model.* **2010**, *29* (1), 93–101, https://doi.org/10.1016/j.jmgm.2010.05.005.
46. Laskowski, R. A.; Swindells, M. B. LigPlot+: Multiple Ligand-Protein Interaction Diagrams for Drug Discovery. *J. Chem. Inf. Model.* **2011**, *51* (10), 2778–2786, https://doi.org/10.1021/ci200227u.
47. Cleves, A. E.; Jain, A. N. Structure- and Ligand-Based Virtual Screening on DUD-E+: Performance Dependence on Approximations to the Binding Pocket. *J. Chem. Inf. Model.* **2020**, *60* (9), 4296–4310, https://doi.org/10.1021/acs.jcim.0c00115.
48. Mysinger, M. M.; Carchia, M.; Irwin, J. J.; Shoichet, B. K. Directory of Useful Decoys, Enhanced (DUD-E): Better Ligands and Decoys for Better Benchmarking. *J. Med. Chem.* **2012**, *55* (14), 6582–6594, https://doi.org/10.1021/jm300687e.
49. López-Ratón, M.; Rodríguez-Álvarez, M. X.; Cadarso-Suárez, C.; Gude-Sampedro, F. OptimalCutpoints: An R Package for Selecting Optimal Cutpoints in Diagnostic Tests. *J. Stat. Softw.* **2014**, *61* (8), 1–36, https://doi.org/10.18637/jss.v061.i08.
50. DeLano, W. Pymol: An Open-Source Molecular Graphics Tool. CCP4 Newsletter on Protein Crystallography No. 700, **2002**.
51. Daina, A.; Michielin, O.; Zoete, V. SwissADME: A Free Web Tool to Evaluate Pharmacokinetics, Drug-Likeness and Medicinal Chemistry Friendliness of Small Molecules. *Sci. Rep.* **2017**, *7* (January), 1–13, https://doi.org/10.1038/srep42717.
52. Kalai, F. El; Çınar, E. B.; Lai, C.-H.; Daoui, S.; Chelfi, T.; Allali, M.; Dege, N.; Karrouchi, K.; Benchat, N. Synthesis, Spectroscopy, Crystal Structure, TGA/DTA Study, DFT and Molecular Docking Investigations of (E)-4-(4-Methylbenzyl)-6-Styrylpyridazin-3(2H)-One. *J. Mol. Struct.* **2021**, *1228*, 129435, https://doi.org/https://doi.org/10.1016/j.molstruc.2020.129435.
53. Lagunin, A.; Stepanchikova, A.; Filimonov, D.; Poroikov, V. PASS: Prediction of Activity Spectra for Biologically Active Substances. *Bioinformatics* **2000**, *16* (8), 747–748, https://doi.org/10.1093/bioinformatics/16.8.747.
54. Jamkhande, P. G.; Pathan, S. K.; Wadher, S. J. *In Silico* PASS Analysis and Determination of Antimycobacterial, Antifungal, and Antioxidant Efficacies of Maslinic Acid in an Extract Rich in Pentacyclic Triterpenoids. *Int. J. Mycobacteriol.* **2016**, *5* (4), 417–425, https://doi.org/10.1016/j.ijmyco.2016.06.020.
55. Wishart, D. S.; Feunang, Y. D.; Guo, A. C.; Lo, E. J.; Marcu, A.; Grant, J. R.; Sajed, T.; Johnson, D.; Li, C.; Sayeeda, Z.; Assempour, N.; Iynkkaran, I.; Liu, Y.; MacIejewski, A.; Gale, N.; Wilson, A.; Chin, L.; Cummings, R.; Le, Di.; Pon, A.; Knox, C.; Wilson, M. DrugBank 5.0: A Major Update to the DrugBank Database for 2018. *Nucleic Acids Res.* **2018**, *46* (D1), D1074–D1082, https://doi.org/10.1093/nar/gkx1037.
56. Wishart, D. S.; Knox, C.; Guo, A. C.; Cheng, D.; Shrivastava, S.; Tzur, D.; Gautam, B.; Hassanali, M. DrugBank: A Knowledgebase for Drugs, Drug Actions and Drug Targets. *Nucleic Acids Res.* **2008**, *36* (Database issue), D901–D906, https://doi.org/10.1093/nar/gkm958.
57. Kumari, R.; Kumar, R.; Lynn, A. G-Mmpbsa -A GROMACS Tool for High-Throughput MM-PBSA

Calculations. *J. Chem. Inf. Model.* **2014**, *54* (7), 1951–1962, https://doi.org/10.1021/ci500020m.

58. Abraham, M. J.; Murtola, T.; Schulz, R.; Pall, S.; Smith, J. C.; Hess, B.; Lindah, E. Gromacs: High Performance Molecular Simulations through Multi-Level Parallelism from Laptops to Supercomputers. *SoftwareX* **2015**, *1–2*, 19–25, https://doi.org/10.1016/j.softx.2015.06.001.
59. Turner, P. XMGRACE, Version 5.1. 19. *Center for Coastal Land-Margin Research, Oregon Graduate Institute of Science and Technology, Beaverton* **2005**, *2* (5), 19, https://doi.org/10.1163/_q3_SIM_00374.
60. Boateng, R. A.; Tastan Bishop, Ö.; Musyoka, T. M. Characterisation of Plasmodial Transketolases and Identification of Potential Inhibitors: An *In Silico* Study. *Malar. J.* **2020**, *19* (1), 1–19, https://doi.org/10.1186/s12936-020-03512-1.
61. Kwofie, S. K.; Dolling, N. N. O.; Donkoh, E.; Laryea, G. M.; Mosi, L.; Miller, W. A.; Adinortey, M. B.; Wilson, M. D. Pharmacophore-Guided Identification of Natural Products as Potential Inhibitors of Mycobacterium Ulcerans Cystathionine γ-Synthase Metb. *Computation* **2021**, *9* (3), 32, https://doi.org/10.3390/computation9030032.
62. Laulumaa, S.; Kursula, P. Sub-Atomic Resolution Crystal Structures Reveal Conserved Geometric Outliers at Functional Sites. *Molecules* **2019**, *24* (17), 3044, https://doi.org/10.3390/molecules24173044.
63. Broni, E.; Ashley, C. N.; Velazquez, M.; Sakyi, P. O.; Kwofie, S. K.; Miller, W. A. Structure-Based Discovery of Potential HPV E6 and EBNA1 Inhibitors: Implications for Cervical Cancer Treatment. *Computation* **2024**, *12*, 112, https://doi.org/10.3390/computation12060112.
64. Zhang, W.; Chipman, P. R.; Corver, J.; Johnson, P. R.; Zhang, Y.; Mukhopadhyay, S.; Baker, T. S.; Strauss, J. H.; Rossmann, M. G.; Kuhn, R. J. Visualization of Membrane Protein Domains by Cryo-Electron Microscopy of Dengue Virus. *Nat. Struct. Biol.* **2003**, *10* (11), 907–912, https://doi.org/10.1038/nsb990.
65. Hu, T.; Wu, Z.; Wu, S.; Chen, S.; Cheng, A. The Key Amino Acids of E Protein Involved in Early Flavivirus Infection : Viral Entry. *Virol. J.* **2021**, *18*, 1–12, https://doi.org/10.1186/s12985-021-01611-2.
66. Sarker, A.; Dhama, N.; Gupta, R. D. Dengue Virus Neutralizing Antibody : A Review of Targets. *Front Immunol.* **2023**, *14*, 1200195, https://doi.org/10.3389/fimmu.2023.1200195.
67. Dubey, K. D.; Tiwari, G.; Ojha, R. P. Targeting Domain-III Hinging of Dengue Envelope (DENV-2) Protein by MD Simulations, Docking and Free Energy Calculations. *J. Mol. Model.* **2017**, *23* (4), 1–8, https://doi.org/10.1007/s00894-017-3259-2.
68. Devadasu, V. R.; Deb, P. K.; Maheshwari, R.; Sharma, P.; Tekade, R. K. Physicochemical, Pharmaceutical, and Biological Considerations in GIT Absorption of Drugs, in *Dosage Form Design Considerations*, Elsevier Inc., 2018, https://doi.org/10.1016/B978-0-12-814423-7.00005-8.
69. Hajian-Tilaki, K. Receiver Operating Characteristic (ROC) Curve Analysis for Medical Diagnostic Test Evaluation. *Casp. J. Intern. Med.* **2013**, *4* (2), 627–635.
70. Goksuluk, D.; Korkmaz, S.; Zararsiz, G.; Karaagaoglu, A. E. EasyROC: An Interactive Web-Tool for Roc Curve Analysis Using R Language Environment. *The R Journal* **2016**, *8* (2), 213–230, https://doi.org/10.32614/rj-2016-042.
71. Dege, N. Experimental and Theoretical Approaches on Structural, Spectroscopic (FT-IR and UV-Vis), Nonlinear Optical, and Molecular Docking Analyses for Zn (II) and Cu (II) Complexes of 6-Chloropyridine-2-Carboxylic Acid. *Appl. Organomet. Chem*. **2022**, *36* (6), 1–16, https://doi.org/10.1002/aoc.6678.
72. Patil, R.; Das, S.; Stanley, A.; Yadav, L.; Sudhakar, A.; Varma, A. K. Optimized Hydrophobic Interactions and Hydrogen Bonding at the Target-Ligand Interface Leads the Pathways of Drug-Designing. *PLoS One* **2010**, *5* (8), e12029, https://doi.org/10.1371/journal.pone.0012029.
73. Mirza, M. U.; Ikram, N. Integrated Computational Approach for Virtual Hit Identification against Ebola Viral Proteins VP35 and VP40. *Int. J. Mol. Sci.* **2016**, *17* (11), 1748, https://doi.org/10.3390/ijms17111748.
74. Kansız, S.; Azam, M.; Basılı, T.; Meral, S.; Aktaş, F. A.; Yeşilbağ, S.; Min, K.; Ağar, A. A.; Dege, N. Synthesis, Structural Studies, Hirshfeld Surface Analysis, and Molecular Docking Studies of a Thiophene-Based Schiff Base Compound. *J. Mol. Struct.* **2022**, *1265*, 133477, / https://doi.org/10.1016/j.molstruc.2022.133477.
75. Şahin, S.; Dege, N. Synthesis, Characterization, X-Ray, HOMO-LUMO, MEP, FT-IR, NLO, Hirshfeld Surface, ADMET, Boiled-Egg Model Properties and Molecular Docking Studies with Human Cyclophilin D (CypD) of a Schiff Base Compound: (E)-1-(5-Nitro-2-(Piperidin-1-Yl)Phenyl)-N-(3-Nitrophenyl)Methanimine. *Polyhedron* **2021**, *205*, 115320, https://doi.org/https://doi.org/10.1016/j.poly.2021.115320.
76. Goel, R. K.; Singh, D.; Lagunin, A.; Poroikov, V. PASS-Assisted Exploration of New Therapeutic Potential of Natural Products. *Med. Chem. Res.* **2010**, *20* (9), 1509–1514, https://doi.org/10.1007/S00044-010-9398-Y.

77. Sinha, S.; Singh, K.; Ravi Kumar, Y. S.; Roy, R.; Phadnis, S.; Meena, V.; Bhattacharyya, S.; Verma, B. Dengue Virus Pathogenesis and Host Molecular Machineries. *J. Biomed. Sci.* **2024**, *31* (1), 1–24, https://doi.org/10.1186/s12929-024-01030-9.
78. Zhou, Z.; Khaliq, M.; Suk, J.-E.; Patkar, C.; Li, L.; Kuhn, R. J.; Post, C. B. Antiviral Compounds Discovered by Virtual Screening of Small–Molecule Libraries against Dengue Virus E Protein. *ACS Chem. Biol.* **2008**, *3* (12), 765–775, https://doi.org/10.1021/cb800176t.
79. de Wispelaere, M.; Lian, W.; Potisopon, S.; Li, P. C.; Jang, J.; Ficarro, S. B.; Clark, M. J.; Zhu, X.; Kaplan, J. B.; Pitts, J. D.; Wales, T. E.; Wang, J.; Engen, J. R.; Marto, J. A.; Gray, N. S.; Yang, P. L. Inhibition of Flaviviruses by Targeting a Conserved Pocket on the Viral Envelope Protein. *Cell Chem. Biol.* **2018**, *25* (8), 1006–1016.e8, https://doi.org/10.1016/j.chembiol.2018.05.011.
80. Modis, Y.; Ogata, S.; Clements, D.; Harrison, S. C. A Ligand-Binding Pocket in the Dengue Virus Envelope Glycoprotein. *Proc. Natl. Acad. Sci.* **2003**, *100* (12), 6986–6991.
81. Panche, A. N.; Diwan, A. D.; Chandra, S. R. Flavonoids: An Overview. *J. Nutr. Sci.* **2016**, *5*, e47, https://doi.org/10.1017/jns.2016.41.
82. Qian, S.; Fan, W.; Qian, P.; Zhang, D.; Wei, Y.; Chen, H.; Li, X. Apigenin Restricts FMDV Infection and Inhibits Viral IRES Driven Translational Activity. *Viruses* **2015**, *7* (4), 1613–1626, https://doi.org/10.3390/v7041613.
83. Wang, L.; Song, J.; Liu, A.; Xiao, B.; Li, S.; Wen, Z.; Lu, Y.; Du, G. Research Progress of the Antiviral Bioactivities of Natural Flavonoids. *Nat. Prod. Bioprospect.* **2020**, *10* (5), 271–283, https://doi.org/10.1007/s13659-020-00257-x.
84. Suroengrit, A.; Yuttithamnon, W.; Srivarangkul, P.; Pankaew, S.; Kingkaew, K.; Chavasiri, W.; Boonyasuppayakorn, S. Halogenated Chrysins Inhibit Dengue and Zika Virus Infectivity. *Sci. Rep.* **2017**, *7* (1), 1–11, https://doi.org/10.1038/s41598-017-14121-5.
85. Loaiza-Cano, V.; Monsalve-Escudero, L. M.; Filho, C. da S. M. B.; Martinez-Gutierrez, M.; de Sousa, D. P. Antiviral Role of Phenolic Compounds against Dengue Virus: A Review. *Biomolecules* **2021**, *11* (1), 1–28, https://doi.org/10.3390/biom11010011.
86. Rothan, H. A.; Mohamed, Z.; Paydar, M.; Rahman, N. A.; Yusof, R. Inhibitory Effect of Doxycycline against Dengue Virus Replication *in Vitro*. *Arch. Virol.* **2014**, *159* (4), 711–718, https://doi.org/10.1007/s00705-013-1880-7.
87. Mazumder, M.; Ponnan, P.; Das, U.; Gourinath, S.; Khan, H. A.; Yang, J.; Sakharkar, M. K. Investigations on Binding Pattern of Kinase Inhibitors with PPAR *γ*: Molecular Docking, Molecular Dynamic Simulations, and Free Energy Calculation Studies. *PPAR Res.* **2017**, *2017*, 6397836, https://doi.org/10.1155/2017/6397836.
88. Musyoka, T. M.; Kanzi, A. M.; Lobb, K. A.; Tastan Bishop, Ö. Structure Based Docking and Molecular Dynamic Studies of Plasmodial Cysteine Proteases against a South African Natural Compound and Its Analogs. *Sci. Rep.* **2016**, *6* (1), 23690, https://doi.org/10.1038/srep23690.
89. Kwofie, S. K.; Dankwa, B.; Enninful, K. S.; Adobor, C.; Broni, E.; Ntiamoah, A.; Wilson, M. D. Molecular Docking and Dynamics Simulation Studies Predict Munc18b as a Target of Mycolactone: A Plausible Mechanism for Granule Exocytosis Impairment in Buruli Ulcer Pathogenesis. *Toxins (Basel)* **2019**, *11* (3), 181, https://doi.org/10.3390/toxins11030181.
90. Agyapong, O.; Asiedu, S. O.; Kwofie, S. K.; Miller, W. A.; Parry, C. S.; Sowah, R. A.; Wilson, M. D. Molecular Modelling and de Novo Fragment-Based Design of Potential Inhibitors of Beta-Tubulin Gene of Necator Americanus from Natural Products. *Informatics Med. Unlocked* **2021**, *26* (February), 100734, https://doi.org/10.1016/j.imu.2021.100734.
91. Kwofie, S. K.; Hanson, G.; Sasu, H.; Enninful, K. S.; Mensah, F. A.; Nortey, R. T.; Yeboah, O. P.; Agoni, C.; Wilson, M. D. Molecular Modelling and Atomistic Insights into the Binding Mechanism of MmpL3 Mtb. *Chem. Biodivers.* **2022**, *19* (9), e202200160, https://doi.org/10.1002/cbdv.202200160.
92. Adinortey, C. A.; Kwarko, G. B.; Koranteng, R.; Boison, D.; Obuaba, I.; Wilson, M. D.; Kwofie, S. K. Molecular Structure-Based Screening of the Constituents of Calotropis Procera Identifies Potential Inhibitors of Diabetes Mellitus Target Alpha Glucosidase. *Curr. Issues Mol. Biol.* **2022**, *44* (2), 963–987, https://doi.org/10.3390/cimb44020064.
93. Liao, K. H.; Chen, K. B.; Lee, W. Y.; Sun, M. F.; Lee, C. C.; Chen, C. Y. C. Ligand-Based and Structure-Based Investigation for Alzheimer's Disease from Traditional Chinese Medicine. *Evidence-based Complement. Altern. Med.* **2014**, *2014*, 364819, https://doi.org/10.1155/2014/364819.
94. Adams, L.; Afiadenyo, M.; Kwofie, S. K.; Wilson, M. D.; Kusi, K. A.; Obiri-Yeboah, D.; Moane, S.; McKeon-Bennett, M. *In Silico* Screening of Phytochemicals from Dissotis Rotundifolia against Plasmodium Falciparum Dihydrofolate Reductase. *Phytomed. Plus* **2023**, *3* (2), 100447, https://doi.org/10.1016/j.phyplu.2023.100447.
95. Ashley, C. N.; Broni, E.; Wood, C. M.; Okuneye, T.; Ojukwu, M. P. T.; Dong, Q.; Gallagher, C.; Miller, W. A.

Identifying Potential Monkeypox Virus Inhibitors: An *in Silico* Study Targeting the A42R Protein. *Front. Cell. Infect. Microbiol.* **2024**, *14* (March), 1–19, https://doi.org/10.3389/fcimb.2024.1351737.

96. Dong, Y. W.; Liao, M. L.; Meng, X. L.; Somero, G. N. Structural Flexibility and Protein Adaptation to Temperature: Molecular Dynamics Analysis of Malate Dehydrogenases of Marine Molluscs. *Proc. Natl. Acad. Sci. U. S. A.* **2018**, *115* (6), 1274–1279, https://doi.org/10.1073/pnas.1718910115.
97. Genheden, S.; Ryde, U. The MM / PBSA and MM / GBSA Methods to Estimate Ligand-Binding Affinities. *Expert Opin. Drug Discov.* **2015**, *10* (5), 449–461.
98. Broni, E.; Kwofie, S. K.; Asiedu, S. O.; Miller, W. A.; Wilson, M. D. A Molecular Modeling Approach to Identify Potential Antileishmanial Compounds against the Cell Division Cycle (Cdc)-2-related Kinase 12 (Crk12) Receptor of Leishmania Donovani. *Biomolecules* **2021**, *11* (3), 1–32, https://doi.org/10.3390/biom11030458.
99. Ganesan, A.; Coote, M. L.; Barakat, K. Molecular Dynamics-Driven Drug Discovery: Leaping Forward with Confidence. *Drug Discov. Today* **2017**, *22* (2), 249–269, https://doi.org/10.1016/j.drudis.2016.11.001.
100. Kwofie, S. K.; Broni, E.; Asiedu, S. O.; Kwarko, G. B.; Dankwa, B.; Enninful, K. S.; Tiburu, E. K.; Wilson, M. D. Cheminformatics-Based Identification of Potential Novel Anti-Sars-Cov-2 Natural Compounds of African Origin. *Molecules* **2021**, *26* (2), 406, https://doi.org/10.3390/molecules26020406.
101. Asiedu, S. O.; Kwofie, S. K.; Broni, E.; Wilson, M. D. Computational Identification of Potential Anti-Inflammatory Natural Compounds Targeting the P38 Mitogen-Activated Protein Kinase (Mapk): Implications for Covid-19-Induced Cytokine Storm. *Biomolecules* **2021**, *11* (5), 653, https://doi.org/10.3390/biom11050653.
102. Adams, L.; Issahaku, A. R.; Agoni, C.; Afiadenyo, M.; Asamoah Kusi, K.; Moane, S.; Obiri-Yeboah, D.; McKeon-Bennett, M. *In Silico* Identification of Potential PvFKBP35 Inhibitors from Entadrophragma Angolense Limonoids Extracts as Antimalarial Agents. *Informatics Med. Unlocked* **2023**, *41* (October), 101319, https://doi.org/10.1016/j.imu.2023.101319.
103. Dankwa, B.; Broni, E.; Enninful, K. S.; Kwofie, S. K.; Wilson, M. D. Consensus Docking and MM-PBSA Computations Identify Putative Furin Protease Inhibitors for Developing Potential Therapeutics against COVID-19. *Struct. Chem.* **2022**, *33* (6), 2221–2241, https://doi.org/10.1007/s11224-022-02056-1.
104. Kielian, M. Class II Virus Membrane Fusion Proteins. *Virology* **2006**, *344* (1), 38–47, https://doi.org/10.1016/j.virol.2005.09.036.